ANL-75-50

ANL-75-50



CHEMICAL ENGINEERING DIVISION

# LIQUID METALS CHEMISTRY AND TRITIUM CONTROL TECHNOLOGY ANNUAL REPORT

July 1974—June 1975

by

V. A. Maroni, C. C. McPheeters, W. F. Calaway,
J. M. McKee, D. J. Raue, S. B. Skladzien,
E. H. Van Deventer, E. Veleckis, R. M. Yonco,
F. A. Cafasso, and L. Burris

U of C-AUA-USERDA

ARGONNE NATIONAL LABORATORY, ARGONNE, ILLINOIS

Prepared for the U. S. ENERGY RESEARCH
AND DEVELOPMENT ADMINISTRATION
under Contract W-31-109-Eng-38

The facilities of Argonne National Laboratory are owned by the United States Government. Under the terms of a contract (W-31-109-Eng-38) between the U. S. Energy Research and Development Administration, Argonne Universities Association and The University of Chicago, the University employs the staff and operates the Laboratory in accordance with policies and programs formulated, approved and reviewed by the Association.

MEMBERS OF ARGONNE UNIVERSITIES ASSOCIATION

The University of Arizona
Carnegie-Mellon University
Case Western Reserve University
The University of Chicago
University of Cincinnati
Illinois Institute of Technology
University of Illinois
Indiana University
Iowa State University
The University of Iowa
Kansas State University
The University of Kansas
Loyola University
Marquette University
Michigan State University
The University of Michigan
University of Minnesota
University of Missouri
Northwestern University
University of Notre Dame
The Ohio State University
Ohio University
The Pennsylvania State University
Purdue University
Saint Louis University
Southern Illinois University
The University of Texas at Austin
Washington University
Wayne State University
The University of Wisconsin



Printed in the United States of America
Available from
National Technical Information Service
U. S. Department of Commerce
5285 Port Royal Road
Springfield, Virginia 22161
Price: Printed Copy $4.00; Microfiche $2.25

Distribution Category:
Chemistry (UC-4)

ANL-75-50

ARGONNE NATIONAL LABORATORY
9700 South Cass Avenue
Argonne, Illinois 60439

CHEMICAL ENGINEERING DIVISION

# LIQUID METALS CHEMISTRY AND TRITIUM CONTROL TECHNOLOGY ANNUAL REPORT

July 1974—June 1975

by

V. A. Maroni, C. C. McPheeters, W. F. Calaway,
J. M. McKee, D. J. Raue, S. B. Skladzien,
E. H. Van Deventer, E. Veleckis, R. M. Yonco,
F. A. Cafasso, and L. Burris

September 1975

Previous reports in this series

| | |
|---|---|
| ANL-7878 | July—December 1971 |
| ANL-7923 | January—June 1972 |
| ANL-7978 | July—December 1972 |
| ANL-8023 | January—June 1973 |
| ANL-8123 | July 1973—June 1974 |

TABLE OF CONTENTS

LIST OF FIGURES

LIST OF TABLES

# CHEMICAL ENGINEERING DIVISION
# LIQUID METALS CHEMISTRY AND TRITIUM CONTROL TECHNOLOGY ANNUAL REPORT
# July 1974-June 1975

by

V. A. Maroni, C. C. McPheeters, W. F. Calaway,
J. M. McKee, D. J. Raue, S. B. Skladzien,
E. H. Van Deventer, E. Veleckis, R. M. Yonco,
F. A. Cafasso, and L. Burris

## ABSTRACT

A program is in progress to develop the capabilities for monitoring hydrogen and tritium in LMFBR sodium and cover gas and to develop means of control of tritium in sodium. The development of the cover-gas hydrogen meter has utilized existing technology from the in-sodium hydrogen meter development. Two of these meters have been fabricated for use on the Core Component Test Loop. Both the in-sodium and cover-gas tritium monitors are similar in design to the hydrogen monitors. The in-sodium tritium monitors have been tested for response to changes in tritium level in sodium. A cover-gas tritium monitor has been designed for testing and further development. Cold-trapping studies have started using an existing cold-trap to determine its effectiveness in removing tritium from sodium. Other cold-trap configurations will be studied including a model of the CRBRP configuration and an analytical cold-trap for more basic studies of precipitation mechanisms.

Physicochemical and thermodynamic studies of liquid lithium-containing systems have continued. Calibration curves for temperature gradient and thermal molecular flow effects in the gravimetric apparatus have been determined and measurements of the uptake of hydrogen by liquid lithium using the gravimetric technique have been initiated. Final results of tensimetric studies of the Li-LiD system are reported. Comparison of the Li-LiD data with previous results for the Li-LiH system shows that the isotope effects in these systems originate largely from the gas phase. An investigation of the solubility of hydrogen in lithium-aluminum alloys has been initiated. The solubility of hydrogen in β-phase Li-Al alloy was found to be significantly lower than that in pure lithium at comparable temperatures and equilibrium hydrogen pressures. The decomposition pressure of nitrogen over $Li_3N$ was measured between 660 and 778°C. These decomposition pressure data, together with previously measured solubilities of $Li_3N$ in liquid lithium were used to determine (1) the equilibrium constant for the formation of $Li_3N_{(s)}$ from liquid lithium and gaseous nitrogen, (2) the free energy of formation of solid $Li_3N$, and (3) the Sieverts' law constant for dilute solutions of $Li_3N$ in liquid lithium.

Work is in progress to develop tritium containment and control methodology that would be applicable to a variety of controlled fusion reactor environments. Studies of the hydrogen permeation characteristics of multiplex metal laminates indicate that these materials may be of potential utility as barriers to tritium migration in heat exchangers and other high-temperature fusion reactor structures. Work performed thus far has demonstrated (1) that the hydrogen permeabilities of these multiplexes obey Fick's Law, (2) that they maintain their integrity in a hydrogen environment, (3) that >50-fold reductions in hydrogen permeabilities (compared to conventional construction materials) are achievable and (4) that fabrication into useful configurations is possible. Studies of the kinetics of chemical trapping reactions involving tritium in inert gas streams show that continuous oxidation of HT to HTO using $CuO/MnO_2$ mixtures and continuous reduction of HTO to HT using magnesium metal can be carried out in small fixed beds under carefully controlled conditions. Progress in the assessment of tritium handling and containment requirements for a tokamak experimental fusion power reactor (TEPR) is reported and a preliminary design description for the TEPR tritium handling facility is given.

## SUMMARY

Hydrogen and Tritium in LMFBR Sodium

The objectives of this program are to develop the capabilities for monitoring both hydrogen and tritium in sodium and in the cover gas, and to study methods including cold-trapping for control of tritium in sodium. Monitors have been developed for measuring hydrogen in cover gas, tritium in sodium, and tritium in cover gas. Development and testing of these meters and the study of tritium removal by cold trapping are the primary efforts of this program.

Cover-Gas Hydrogen Meter Development. Existing technology from the in-sodium hydrogen-meter development was used as the starting point for development of the cover-gas hydrogen meter. This meter operates by diffusion of hydrogen through a nickel membrane and direct measurement of the equilibrium hydrogen pressure. Two meters of this type were fabricated for testing and further development on the Apparatus for Monitoring and Purifying Sodium (AMPS). Three advanced meters of this type were fabricated, one for use by the Components Technology Division in their studies of sodium-water reaction, and two to replace the two earlier models in use on AMPS.

Tritium Monitoring in LMFBR Sodium. Tritium monitor development work has been done with the Apparatus for Monitoring and Purifying Sodium (AMPS). AMPS has been upgraded by the addition of cover-gas access ports and improvements of several minor features. Two in-sodium tritium monitors have been tested to confirm their proper operation, and a cover-gas tritium monitor has been designed and is being fabricated. Two additional in-sodium tritium monitors are being built for installation on the EBR-II primary and secondary sodium systems.

Tritium Control in LMFBR Sodium. The primary method for tritium control in LMFBR sodium currently under development is cold-trapping. The first cold-trapping studies are being performed with the existing experimental cold trap on AMPS. Future cold-trapping studies will be done using a model of the Clinch River Breeder Reactor Plant cold-trap and an analytical cold trap designed for more basic studies of precipitation mechanisms. The efficiency of these cold traps for removing tritium from sodium will be measured under conditions of coprecipitation of hydrogen with tritium and of exchange between tritium in solution with hydrogen as hydride deposits in the cold trap.

## Physicochemical and Thermodynamic Studies of Lithium-Containing Systems

Gravimetric Studies of Hydrogen-Liquid Metal Systems. Gravimetric studies to obtain temperature-pressure-composition data on Li-LiH and Li-LiD below the respective monotectic temperatures are being reinitiated. Preliminary experiments have been completed which examined the effect of thermal molecular flow on the microbalance. Calibration curves which account for the temperature differences between the sample capsule and its surroundings have been constructed.

The Lithium-Lithium Deuteride System. The previously reported raw data for the Li-LiD system were refined in a manner already described for the Li-LiH system. The corrected data were fitted to analytical expressions for the activity coefficients of each species. The miscibility-gap boundaries, plateau dissociation pressure, equilibrium constant, and Sieverts' law constant were also represented in analytical forms. A pronounced D/H isotope effect is apparent from the dissociation pressures. For example, between 705 and 871°C, the plateau pressure ratios ($P_{D_2}/P_{H_2}$) varied from 1.40 to 1.35. Since both systems produced essentially identical miscibility gaps, the isotope effect appears to reside principally in the gas phase.

Solutions of Hydrogen in the β-Phase of the Li-Al System. A study of the Li-Al-$H_2$ system was initiated to investigate the interaction between hydrogen and the β-phase (48-56 at. % Li) by measuring the dissociation pressure, P, of hydrogen over solid solutions of hydrogen in the β-phase as a function of temperature, hydrogen concentration, C, and alloy composition. Isotherms of $\sqrt{P}$ *vs.* C measured at 551 and 599°C with an Al-52.9 at. % Li alloy indicate the existence of a wide miscibility gap from 6 to 33 at. % H and the possibility of another, narrower gap existing at lower concentrations (<1 at. % H) below 500°C. Plateau pressures measured for 13.5 at. % H alloy agree with those reported for the last stage in the thermal decomposition of $LiAlH_4$.

Studies of the Solubility of $Li_3N$ in Liquid Lithium and the Thermal Decomposition of $Li_3N$. The melting point (813 ± 1°C) and the decomposition pressures of solid $Li_3N$ at temperatures ranging from 660 to 778°C were measured during this period. The measured decomposition pressures in conjunction with available solubility data permit the calculation of the thermodynamic properties of the lithium-lithium nitride system. The equilibrium constant, K, for the reaction, 3 Li(soln) + 1/2 $N_2$(g) $\rightleftarrows$ $Li_3N$(s), and the

standard free energy of formation of solid $Li_3N$, $\Delta G_f^\circ$, are given by the expressions

$$\ln K \text{ (atm}^{-1/2}) = 16.73 + 19{,}670\ T^{-1}$$

$$\Delta G_f^\circ \text{ (kcal/mol)} = 33.2 \times 10^{-3} T - 39.1$$

The values of the standard entropy and standard enthalpy terms (from the expression for $\Delta G_f^\circ$) are supported by recent calorimetric work and are to be preferred over currently published JANAF values. The Sieverts' law constant for dilute solutions of $Li_3N$ in lithium and the activity coefficients for solute $Li_3N$ and solvent lithium were also calculated.

## Tritium Containment and Control Technology for Fusion Reactors

Experimental Studies of Tritium Barrier Concepts for Fusion Reactors. The hydrogen permeation characteristics of a series of metallurgically bonded metal composites have been investigated. Results for a 316-SS/Cu/316-SS composite and a 304-SS/Cu/Nb composite were in reasonably good agreement with predicted hydrogen permeabilities based on the known permeabilities of the individual layer materials and the application of Fick's law for diffusion. Small differences between measured and observed permeabilities were attributed to effects occuring at the metallurgical interfaces. The integrity of the composites studied was found to be unaffected by large-scale hydrogen throughput. The hydrogen permeability of a copper-aluminum-iron alloy (Cu-10 wt % Al-4 wt % Fe) was found to be over a factor of 40 lower than that of pure copper. Use of this alloy in stainless steel-clad multiplexes could give rise to a >50-fold reduction in tritium migration due to permeation. A 304-SS/Cu/304-SS mechanically bonded multiplex was prepared in seamless tube form and contiguous welding of two sections of this tubing (layer to corresponding layer) to form a liner joint was demonstrated.

Tritium Trapping Kinetics in Inert Gas Streams. An apparatus was assembled to study the kinetics of chemical trapping reactions involving tritium in inert gas streams (*e.g.*, helium, argon, nitrogen) under conditions that are representative of environments anticipated for fusion power reactors. Mixtures of CuO and $MnO_2$ were found to be very effective in converting HT to HTO. At temperatures between 580°C and 610°C, magnesium metal was found to be somewhat effective in converting HTO back to HT. A liquid nitrogen-cooled copper mesh trap was very effective in removing HTO from helium purge streams without simultaneously removing HT. Liquid-nitrogen-cooled #5A molecular sieve effectively removed both HT and HTO from helium purge streams, but its capacity to remove HT diminished rapidly with increased trap loading.

Assessment of the Tritium Handling and Containment Requirements for a Tokamak Experimental Power Reactor. An effort is under way to assess the tritium handling and containment requirements for an experimental fusion power reactor (TEPR) based on the tokamak confinement concept. The tritium-handling facility for the initial stage of operation of the TEPR has been broken down into six major systems: fuel-delivery, fuel-circulation, fuel-

processing, fuel-storage, inplant-containment, and purge-processing. A later stage of operation, involving implementation of a lithium-containing blanket material to test tritium-breeding performance, will require an additional system to provide for blanket processing.

# I. HYDROGEN AND TRITIUM IN LMFBR SODIUM

Monitoring and control of both hydrogen and tritium are important in the operation of liquid-metal-cooled fast-breeder reactors (LMFBRs). Hydrogen monitoring is important primarily from the standpoint of detection of water-to-sodium or steam-to-sodium leaks in steam generators, and for determining hydrogen concentration to better understand the interaction between hydrogen and tritium. To minimize the release of tritium to the environment, it is necessary to control the tritium concentration in the sodium and to monitor the concentrations of tritium in the primary and secondary sodium coolant streams.

The objectives of this program are to develop the capabilities for monitoring hydrogen and tritium, both in sodium and in the cover-gas, and to study cold trapping as a means of hydrogen and tritium control in sodium. When hydrogen and tritium are both present in sodium, the cold trap removes both isotopes by simultaneous precipitation of the NaH and NaT; however, when the hydrogen has been removed down to its solubility level as determined by the minimum cold-trap temperature, isotopic exchange between tritium in the sodium stream and hydrogen precipitated in the cold trap must be relied upon for tritium control. Both of these phenomena, coprecipitation and isotopic exchange, are being studied to determine their effectiveness in tritium control in sodium. The tritium and hydrogen monitors will be used to measure the effectiveness of cold-traps for tritium removal.

## A. Cover-Gas Hydrogen Meter Development (S. Skladzien, J. McKee, and D. Raue)

The objective of this part of the program is to develop an instrument for continuous monitoring of the hydrogen content of argon cover-gas in LMFBR sodium systems. Development of the meter includes design, fabrication, and testing at Argonne National Laboratory (ANL). Incorporation of such meters into LMFBR steam-generator leak-detection systems is expected to be a part of other programs.

In the development of the cover-gas hydrogen meter (CGHM), existing in-sodium hydrogen-detector technology[1,2] is being utilized. The meter is an equilibrium diffusion-type monitor with a direct pressure readout that can be related to the partial pressure of hydrogen in the cover-gas.

Figure 1 is a schematic drawing of the CGHM (Mark II design). The principal components of the meter are the nickel diffusion membrane, heater, thermal shield, a pressure-measuring device such as a hot cathode-triode ion gauge, and an ion pump vacuum system for periodic pumpdown. The cover-gas hydrogen meter differs from the ANL in-sodium hydrogen meter in that the former has its own heat source and temperature controller. These features allow the user to maintain the nickel diffusion membrane of the CGHM at any temperature greater than the temperature existing in the cover-gas space. The heater used is in the form of a coil approximately 4 in. (10.16 cm) long by 3/4 in. (1.9 cm) I.D. This heater coil is surrounded by a cylindrical double-walled thermal shield which has an evacuated space between the two walls. With this configuration, the nickel membrane, which is centrally located within the heater coil, is heated mainly by radiation. A continuous flow of cover-gas past the diffusion membrane results from the "chimney effect" produced as the heated gas surrounding the membrane rises; the gas, at the lower temperature

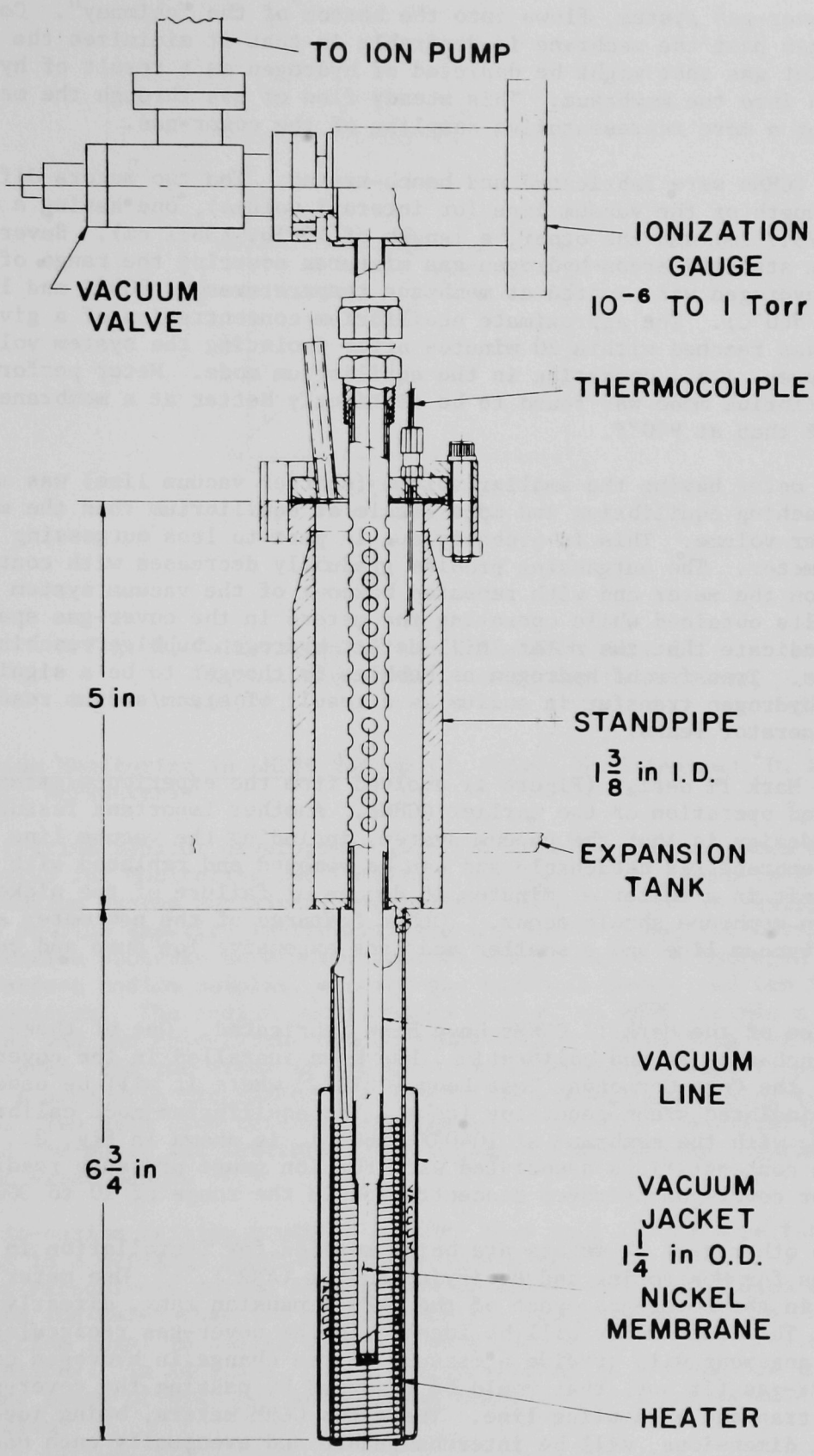


Fig. 1. Hydrogen Meter, Mark II

of the cover-gas system, flows into the bottom of the "chimney". Continuous flow of gas past the membrane is desirable in that it minimizes the possibility of stagnant gas that might be depleted of hydrogen as a result of hydrogen diffusion into the membrane. This steady flow of gas through the meter also allows for a more representative sampling of the cover-gas.

Two CGHMs were fabricated and bench-tested. The two meters differed only in the length of the vacuum line (or internal volume), one having a length of 29 in. (73.7 cm) and the other, a length of 15 in. (38.1 cm). Several different standard argon-hydrogen gas mixtures covering the range of 14 ppm to 220 ppm hydrogen were tested at membrane temperatures of 900°F and 1040°F (482 and 560°C). The approximate equilibrium concentration of a given gas mixture was reached within 20 minutes after isolating the system volume from the ion pump, i.e., operating in the equilibrium mode. Meter performance in the equilibrium mode was found to be distinctly better at a membrane temperature of 1040°F than at 900°F.

The meter having the smaller volume (shorter vacuum line) was more rapid in approaching equilibrium and more stable at equilibrium than the meter with the larger volume. This is probably due in part to less outgassing in the smaller meter. The outgassing problem gradually decreases with continuous pumping on the meter and with repeated bakeout of the vacuum system at 600-700°F. The results obtained while operating the meters in the cover-gas space over sodium indicate that the meters will detect hydrogen bubbles reaching the cover-gas. Transfer of hydrogen as bubbles is thought to be a significant mode of hydrogen transfer in sodium as a result of steam/sodium reactions in steam-generator leaks.

The Mark II design (Figure 1) evolved from the experience gained in the design and operation of two earlier CGHMs. Another important feature of the Mark II design is that the vacuum system, including the vacuum line and nickel membrane, is detachable and can be removed and replaced with a new vacuum unit in a matter of minutes if damage or failure of the nickel diffusion membrane should occur. Other features of the new meter are a shorter vacuum line and a smaller and less expensive ion pump and pump control unit.

Three of the Mark II CGHMs have been fabricated. One of these units, after bench-testing and calibration, has been installed in the cover-gas space of the Core Component Test Loop (CCTL),[3] where it will be used to detect simulated steam-generator leaks. The equilibrium-mode calibration for the CGHM, with the membrane at 1040°F (560°C), is shown in Fig. 2. The hydrogen concentrations associated with the ion gauge pressure readings are shown for cover-gas hydrogen concentration in the range of 10 to 300 vppm.

The other Mark II meters are being readied for installation in the Apparatus for Monitoring and Purifying Sodium (AMPS).[4,5] One meter will be located in the cover-gas space of the AMPS expansion tank, directly over sodium. The other meter will be located in the cover-gas recirculation line. This arrangement will provide a measure of the change in hydrogen content of the cover-gas (if any) that would be produced by passing the cover-gas through a vapor trap and a sampling line. These two CGHM meters, being identical in physical dimensions, will be interchangeable and eventually each one will be used or tested in both locations.

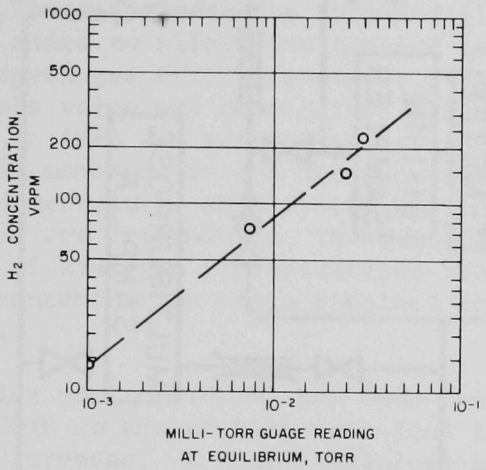


Fig. 2. Calibration of the CCTL CGHM, Mark II (Equilibrium Mode). Membrane temperature, 1040°F.

B. Tritium Monitoring in LMFBR Sodium (J. McKee, S. Skladzien, D. Raue, and C. McPheeters)

The tritium monitor development work performed at ANL has been done in the Apparatus for Monitoring and Purifying Sodium (AMPS). AMPS is a recirculating sodium system containing 100 gallons of sodium and is equipped with extensive on-line impurity instrumentation and impurity control devices. The instrumentation includes an electrochemical oxygen meter, a hydrogen meter, a multi-purpose sodium sampler, a cover-gas hydrogen meter, and two in-sodium tritium monitors. The sodium purification devices on AMPS include a hydrogen getter trap and two cold-traps--one of which is for controlling the system impurity level, and the other is intended for experimental cold-trapping studies. A schematic diagram of the AMPS flow pattern and piping is shown in Fig. 3. Two main flow circuits are provided--one for conditioning the sodium and the other for monitoring the purity and performing impurity-precipitation experiments.

The in-sodium tritium monitors on AMPS were used in tests performed previously in a separate program. These meters were developed by R. Kumar[6,7] and tested extensively in the AMPS sodium to which tritium had been added. These tests indicated that the response of the tritium monitors to changes in the tritium level in sodium was in good agreement with that predicted by calculations. In addition, the hydrogen/tritium ratio remained constant over a wide range of hydrogen and tritium concentrations during cold trapping of the sodium.

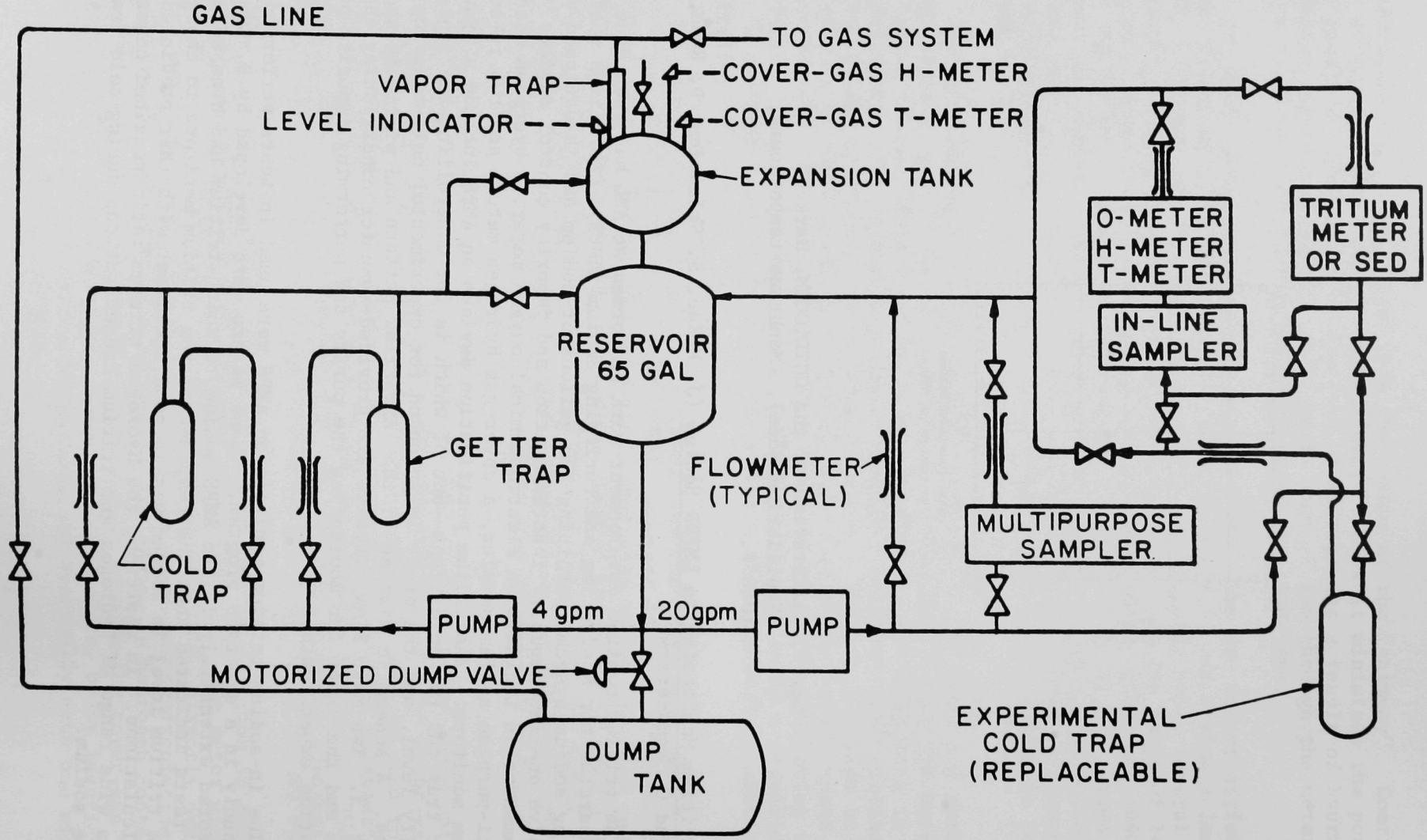


Fig. 3. AMPS Schematic Diagram

A significant part of the revitalization of the tritium monitoring and control program has been the repair and improvement of the AMPS facility. Replacement of a failed dump valve motor required shutdown of the system. During this shutdown period, many improvements were made that allow much more efficient operation. These improvements included (1) two access ports in the cover-gas region were added to allow simultaneous testing of a cover-gas hydrogen meter and a cover-gas tritium monitor; (2) a cold trap bypass line containing an inoperable valve was eliminated; (3) one of two specimen equilibration devices on AMPS was removed and transferred for use on EBR-II; and (4) a faulty nickel membrane in the hydrogen meter was replaced. After these extensive improvements, the AMPS system was restarted and the behavior of the various monitors was determined. The tritium monitors performed as expected over a range of hydrogen concentrations from 1 ppm to 3 ppm, and the hydrogen/tritium concentration ratio remained constant over the various concentration changes.

A cover-gas tritium monitor (CGTM) has been designed for testing in the AMPS cover-gas. The CGTM is essentially identical to the CGHM (see Fig. 1) with two important differences. A small stainless steel tube is inserted into the lower end of the nickel membrane tube so that an argon-plus-hydrogen sweep gas may be passed over the inner membrane surface. A small thermocouple is inserted into the tube to allow more sensitive measurements of the temperature in the region of the nickel membrane.

Two of these CGTMs are being fabricated. One will be inserted directly into the cover-gas space over the sodium, and the other meter will be placed in the argon recirculation system. This arrangement will allow a determination of the effect (if any) of passage of cover-gas through a vapor trap and a length of room-temperature tubing on the tritium concentration of the cover-gas. After these meters are fully developed, two units will be assembled for use in the cover-gas spaces of both the primary and secondary systems of EBR-II.

Three in-sodium tritium monitors (ISTMs) are being fabricated, two for the use on EBR-II and one for transfer to HEDL. These ISTMs are designed to fit within the Westinghouse Model III oxygen-meter housings.[8] Both the primary and secondary sodium systems of EBR-II and a sodium system at HEDL are already equipped with these oxygen-meter housings, so that installation of the ISTMs at these locations will be relatively simple. The nickel membrane of the ISTM extends into the flowing sodium stream inside the oxygen-meter housing. However, the surface area available within the housing is limited and, as a result, the sensitivity of the ISTM will be lower than could be achieved in more available space. A meter with a larger surface area will be designed if reactor experience indicates that the need for such a meter exists.

C. Tritium Control in LMFBR Sodium (J. McKee, S. Skladzien, D. Raue, and C. McPheeters)

The primary method currently conceived for control of tritium in LMFBR sodium is cold trapping. Although cold traps have been used for many years to control impurity levels in sodium systems, little is understood about the behavior of tritium relative to other impurity species in cold traps. When hydrogen and tritium are present in abundant quantities in sodium, they appear

to be precipitated simultaneously with high efficiency in a cold trap. However, when the hydrogen concentration is very low, the presence of very high activity levels of tritium has a negligible effect on the concentration levels of the hydrogen isotopes in the sodium. Under these conditions, the only mechanism available for tritium removal by the cold trap is isotopic exchange between tritium and hydrogen in the cold trap. The purpose of the tritium control program is to study the coprecipitation and isotopic exchange mechanisms independently.

The first cold-trapping studies are being performed using the existing experimental cold trap on the AMPS system (see Fig. 3). Future tritium trapping experiments will be performed using specially designed traps for either collecting and analyzing specific impurities or for modeling certain full-scale cold-trap designs. Of the latter type, a model of the crystallizer tank planned for the secondary sodium system of the Clinch River Breeder Reactor Plant has been designed and is being built. This model will be the first of several cold-trap configurations to be tested on AMPS. Subsequent traps will be designed for more basic cold-trapping studies aimed at more fully understanding the mechanisms of coprecipitation and isotopic exchange in tritium control by cold-trapping.

# II. PHYSICOCHEMICAL AND THERMODYNAMIC STUDIES OF LITHIUM-CONTAINING SYSTEMS

The work described in this section embodies a family of studies on lithium-containing systems pertinent to controlled thermonuclear research. Previous progress reports in the series covering this work are given in references 9, 10, and 11. Reported below are results of (1) an effort to complete the development of a gravimetric technique for the determination of pressure-composition isotherms of hydrogen-liquid metal systems, (2) the final stages of tensimetric studies of the Li-LiD system, (3) initial tensimetric investigations of the Li-Al-$H_2$ system, and (4) investigations of the thermal decomposition of solid $Li_3N$ and their implications with regard to the thermodynamic properties of the Li-$Li_3N$ system.

## A. Gravimetric Studies of Hydrogen-Liquid Metal Systems (W. F. Calaway)

Several years ago, gravimetric experiments were initiated in this laboratory to determine pressure-composition isotherms for the Li-LiH and Li-LiD systems below the respective monotectic temperatures.[9,10] The impetus of this program was to develop a rapid method for data accumulation in liquid metal-hydrogen systems by bringing liquid metal samples, sealed in capsules permeable to hydrogen, into rapid equilibrium with gaseous hydrogen. A gravimetric apparatus meets this criterion since the hydrogen pressure in this type of experiment can be easily and rapidly manipulated to increase the rate of diffusion through the capsule walls.

In the experiment, an automatic recording vacuum microbalance is used to measure weight changes of an encapsulated lithium sample as a function of hydrogen pressure. These weight changes are a direct measure of shifts in the Li-LiH equilibrium along the composition axis. Preliminary results for the Li-LiH system and a description of the experimental procedure have been reported.[9] Since then, a more sensitive microbalance (Cahn R-100) and a new mercury manostat have been installed. A schematic diagram of the updated experimental apparatus is shown in Fig. 4. In addition, the previously used iron sample capsules[10] have been replaced by more permeable (to hydrogen) niobium-1% zirconium capsules.

The previous preliminary study identified two problem areas of the gravimetric experiment which merit detailed consideration before full-scale experiments are begun. They are (1) a temperature gradient that may exist between the sample and its surroundings and (2) thermal molecular flow effects. These two potential problems have been explored in recent months, and progress toward understanding them is summarized below.

### 1. Temperature Effects in the Gravimetric Apparatus

Accurate temperature measurements in gravimetric experiments are difficult since it is not often possible to have thermal contact between the sample and the temperature probe. For this particular experiment, it is impractical to place thermocouples inside the hangdown tube since hydrogen can alter the calibration of certain thermocouples. Temperature gradients exist between the sample capsule and its surroundings so that when thermocouples are placed outside the hangdown tube, it is necessary to apply a correction to

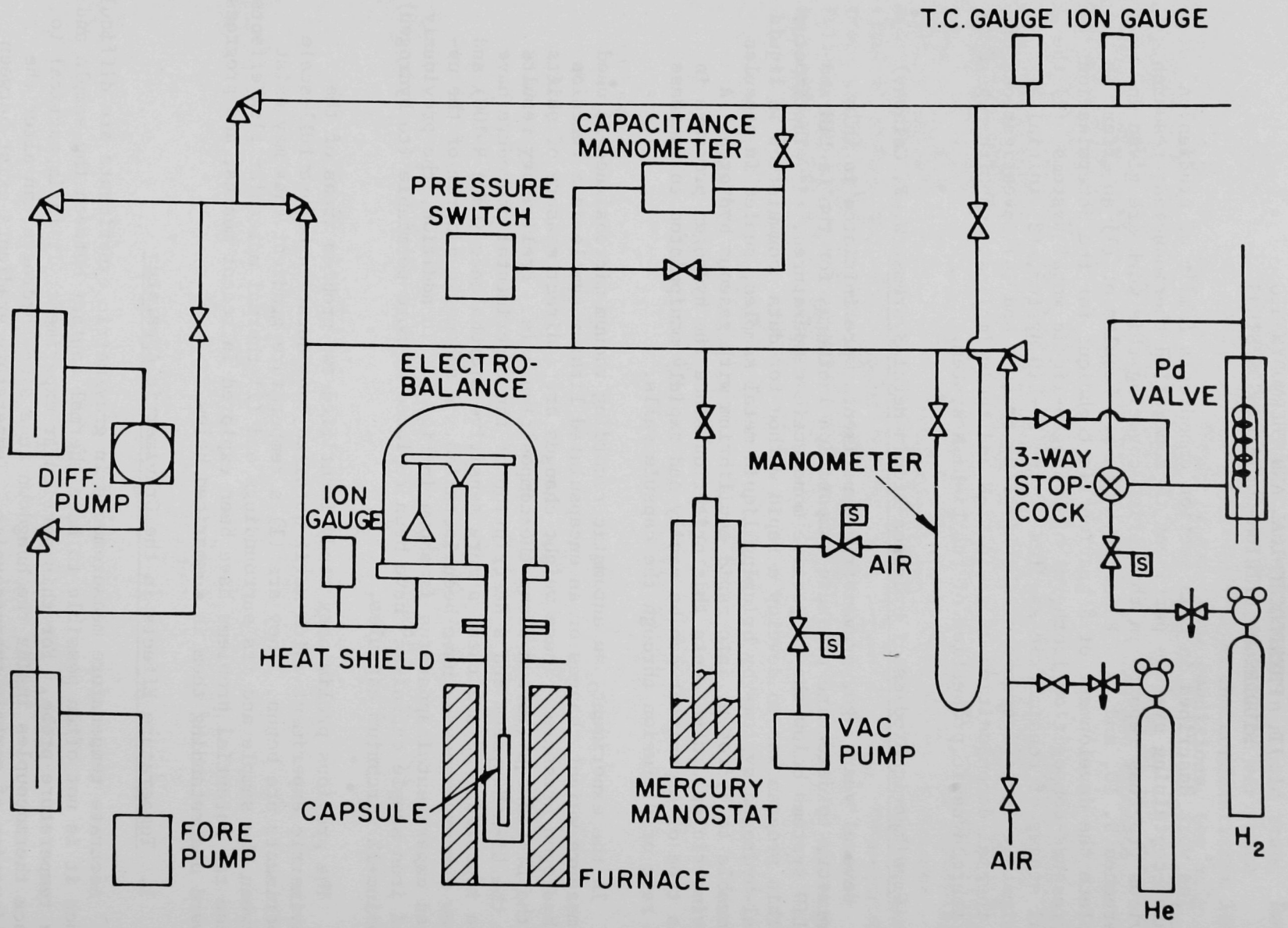


Fig. 4. Schematic Diagram of the Present Gravimetric Experimental Apparatus

the measured temperature. The magnitudes of these correction factors have been determined for the apparatus. This was accomplished by comparing the temperature of a sample capsule which contains a thermocouple with the exterior temperature of the hangdown tube over a wide range of pressures and temperatures.

Three quartz wells were attached to the outside of the hangdown tube. They were positioned radially 120° from each other. One well was placed at the same height as the capsule while the other two were placed at heights above and below the capsule by two inches. Shielded chromel-alumel thermocouples were inserted in the wells which were subsequently filled with alumina. A calibrated Pt/Pt-10%Rh thermocouple was inserted in an alumina-filled quartz tube which was then lowered into a sample capsule containing tin metal. The capsule was suspended in the hangdown tube at the same height as that to be used in the actual experiments.

The hangdown tube and capsule were heated overnight to 300°C. The voltages of the four thermocouples (three exterior to the tube and one in the sample capsule) were recorded at different helium pressures. At each pressure setting, the apparatus was allowed to stand for approximately one hour. This procedure was repeated at 50°C intervals between 300°C and 800°C. To explore the possibility that heat was conducted up the thermocouple insulation tube, thus biasing the results, two tubes of different diameters were used in the experiments. Also, hydrogen was used in two experiments to confirm that hydrogen and helium produce the same temperature differences.

To obtain the desired calibration curves, a correction factor, $\Delta T$, was calculated by subtracting the temperature of the thermocouple in the capsule from the average temperature of the exterior thermocouples for each pressure-temperature combination. Typical data are given in Fig. 5. As is shown, the sample capsule can be colder than the hangdown tube by as much as 10°C or warmer by as much as 2°C depending upon the pressure and temperature.

Additional experiments were performed where the temperature gradient of the hangdown tube was altered by shunting part of the furnace windings. It was found that this changed the temperature difference in an unpredictable manner by as much as 4°C. Thus, it will be critical to control the temperature gradient during experiments.

2. Thermal Molecular Flow Effects

Of major concern in all gravimetric experiments is thermal molecular flow (TMF).[12] It has been demonstrated for systems similar to ours that TMF will cause the apparent weight of a sample as measured by the balance to be altered, thus producing anomalous results. The magnitude of this effect is dependent upon (1) the pressure of the gas, (2) the temperature gradients along the hangdown wire and sample capsule, and (3) the size and shape of the capsule and wire.

Although TMF is well understood, the lack of detailed information on the temperature profile along the balance as well as geometric considerations make a correction to the measured weight from first principles impractical. The usual solution to this problem is to apply an empirical correction factor. These corrections are determined by recording changes in the effective weight of a "dummy" capsule as a function of temperature, temperature gradient, and pressure.

"a"

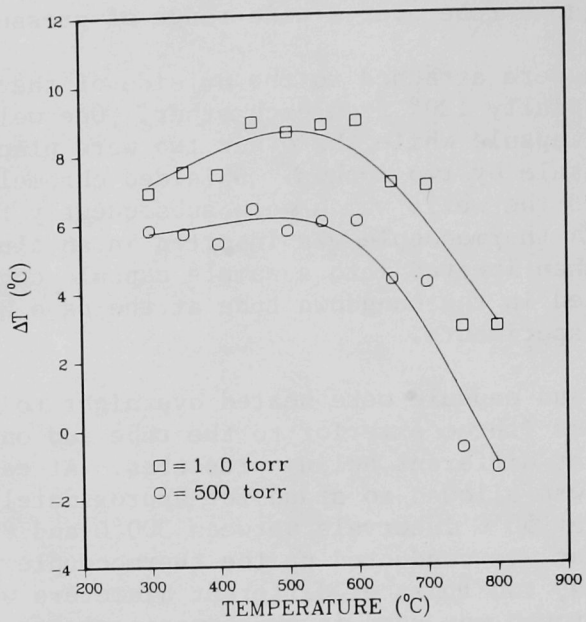


"b"

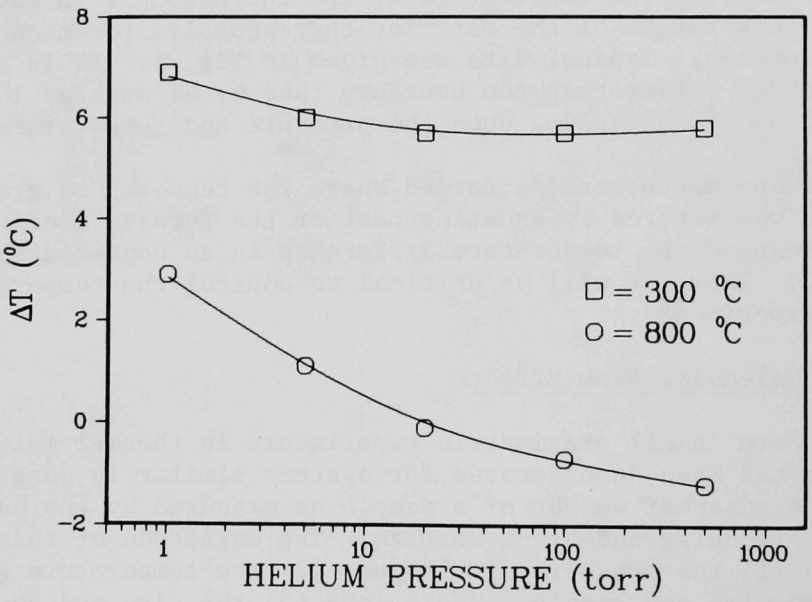


Fig. 5. Typical temperature calibration curves for the gravimetric experiment at constant pressure (Fig. 5a) and temperature (Fig. 5b). ΔT is defined as the temperature difference between the hangdown tube and the sample capsule

To study TMF effects in our apparatus, a platinum tube similar in diameter and length to the niobium sample capsules was suspended from the balance. Helium was used in lieu of hydrogen for these experiments. Calibration curves were constructed by varying the helium pressure over the range 0.0 Torr to 200 Torr at 100°C temperature intervals between 350°C and 750°C. The correction factor, ΔW, was calculated at each temperature by subtracting the observed weight at the given pressure from the weight at zero pressure. Results for the two extreme temperatures studied (350°C and 750°C) are presented in Fig. 6.

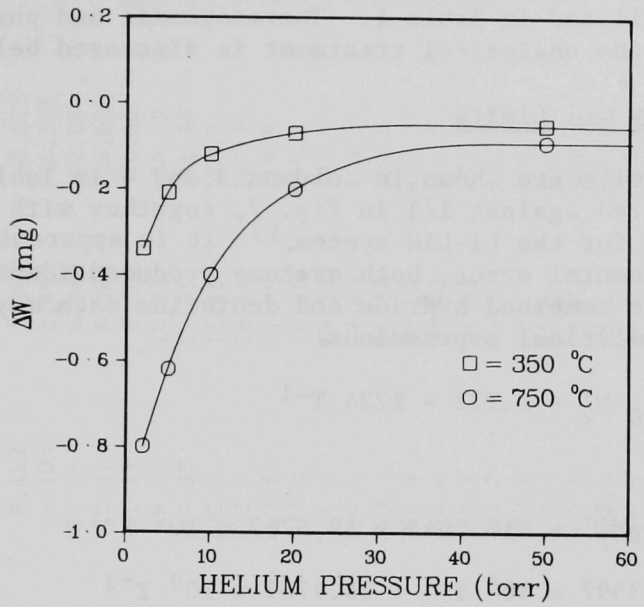


Fig. 6. The Weight Change, ΔW, Due to Thermal Molecular Flow (TMF) as a Function of Pressure at 350°C and 750°C

To determine the reproducibility of the correction factor, two runs with identical temperature gradients at each temperature were performed. In addition, several runs were carried out with the temperature gradient altered. It was found that the reproducibility of ΔW was good as long as the temperature gradient remained unchanged.

It is evident from these preliminary studies that corrections must be applied to both the measured weight and the temperature. Calibration curves for this purpose have been constructed. These corrections were found to be reproducible and, thus, the calibration curves will accurately determine the sample temperature and weight for the gravimetric experiment.

B. The Lithium-Lithium Deuteride System (E. Veleckis)

Progress in the tensimetric studies of the Li-LiD system has been discussed in a previous report.[11] The primary data were shown graphically in the form of five isotherms (at 705, 756, 805, 840, and 871°C) where the square root of deuterium pressure was plotted against composition. Each of the isotherms contained two rising portions that were separated by a horizontal line. The composition ranges of the first and second rising portions correspond to homogeneous phases; the constant-pressure plateau defines the

two-phase coexistence region, the boundaries of which were essentially identical to those of the Li-LiH system.[13] Plateau pressures, determined as a function of temperature in a separate experiment, were also graphically shown.

During the past year, the Li-LiD data were refined in a manner already described for the Li-LiH system,[13] *i.e.*, (1) by applying necessary corrections to the raw data and (2) by fitting the corrected data to analytical expressions for the chemical potentials and activity coefficients of each species. The corrected data are listed in Table 1. Thermodynamic and phase information that resulted from the analytical treatment is discussed below.

1. Miscibility Gap Limits

The amended limits are shown in columns 3 and 4 in Table 2, and their logarithms are plotted against 1/T in Fig. 7, together with the limits previously measured for the Li-LiH system.[13] It is apparent from the graphs that, within experimental error, both systems produced identical miscibility gap boundaries. The combined hydride and deuteride data may be represented by the following analytical expressions:

$$\log_{10} N_2' = 1.122 - 1724\ T^{-1} \tag{1}$$

and

$$\log_{10} N_2'' = -16.5044 + 49.8767 \times 10^3\ T^{-1} - 50.3592 \times 10^6\ T^{-2} + 16.9769 \times 10^9\ T^{-3} \tag{2}$$

where $N_2'$ and $N_2''$ are the mole fractions of the solute species (LiH or LiD) at the lower and upper boundaries, respectively. One datum point (710°C, 25.2 mol % LiH) of the Li-LiH system fell outside the error band and was omitted from the least-squares analysis.

2. Plateau Dissociation Pressures

Deuterium pressures measured over Li-LiD alloys (containing 60-70 mol % LiD) above and below the monotectic temperature are listed in Table 3. The data were fitted to linear equations by the method of least squares. Thus, below the monotectic

$$\ln P_{D_2}\ (\text{Torr}) = 28.073 - 23{,}539\ T^{-1} \tag{3}$$

and above the monotectic

$$\ln P_{D_2}\ (\text{Torr}) = 21.213 - 16{,}940\ T^{-1} \tag{4}$$

The crossing point of the regression lines occurs at 689°C and 36.7 Torr, corresponding to the monotectic temperature and the plateau dissociation pressure at that temperature.

TABLE 1. Pressure-Composition Data for Five Isotherms in the Li-LiD System

| 705°C | | 756°C | | 805°C | | 840°C | | 871°C | |
|---|---|---|---|---|---|---|---|---|---|
| $100\ N_{LiD}$ (Mol % LiD) | $P_{D_2}$ (Torr) | $100\ N_{LiD}$ (Mol % LiD) | $P_{D_2}$ (Torr) | $100\ N_{LiD}$ (Mol % LiD) | $P_{D_2}$ (Torr) | $100\ N_{LiD}$ (Mol % LiD) | $P_{D_2}$ (Torr) | $100\ N_{LiD}$ (Mol % LiD) | $P_{D_2}$ (Torr) |
| 1.113 | 0.200 | 1.154 | 0.367 | 0.972 | 0.482 | 1.057 | 0.873 | 1.544 | 2.06 |
| 2.534 | 1.056 | 2.703 | 2.006 | 2.790 | 4.103 | 2.492 | 4.591 | 3.778 | 12.48 |
| 4.220 | 2.891 | 4.329 | 5.216 | 4.684 | 11.26 | 4.248 | 12.69 | 6.195 | 32.70 |
| 6.234 | 6.154 | 6.304 | 11.10 | 6.468 | 20.72 | 6.305 | 26.69 | 8.697 | 61.79 |
| 8.545 | 11.03 | 8.283 | 18.45 | 8.177 | 31.77 | 8.292 | 44.10 | 11.34 | 100.0 |
| 11.00 | 17.22 | 11.10 | 31.56 | 10.42 | 49.09 | 10.27 | 64.79 | 13.82 | 141.0 |
| 13.54 | 24.18 | 14.49 | 49.39 | 13.00 | 71.87 | 12.55 | 91.94 | 16.86 | 197.2 |
| 16.14 | 32.90 | 18.16 | 71.20 | 15.95 | 100.9 | 15.10 | 125.3 | 20.75 | 271.6 |
| 18.69 | 39.87 | 21.92 | 92.16 | 19.07 | 130.5 | 18.16 | 167.7 | 25.15 | 354.9 |
| 21.43 | 46.48 | 25.34 | 105.2 | 22.39 | 163.8 | 21.78 | 219.9 | 29.58 | 454.0 |
| 24.18 | 48.58 | 32.88 | 114.8 | 26.10 | 197.8 | 26.20 | 291.6 | 34.99 | 536.6 |
| 36.34 | 50.64 | 48.11 | 115.6 | 30.17 | 228.6 | 29.53 | 333.3 | 41.54 | 596.9 |
| 47.90 | 49.20 | 61.86 | 115.6 | 37.66 | 239.4 | 33.41 | 373.3 | 54.75 | 603.2 |
| 96.44 | 47.78 | 86.97 | 115.7 | 53.97 | 243.7 | 61.31 | 400.8 | 75.13 | 606.2 |
| 97.88 | 49.30 | 91.51 | 115.8 | 64.52 | 245.4 | 89.22 | 403.3 | 90.74 | 607.8 |
| 98.45 | 66.76 | 96.19 | 116.2 | 88.99 | 244.6 | 92.42 | 404.4 | 92.06 | 624.2 |
| 98.81 | 98.72 | 97.35 | 122.3 | 90.53 | 246.3 | 94.01 | 425.5 | 92.92 | 658.8 |
| 99.05 | 141.2 | 98.14 | 173.4 | 92.40 | 245.7 | 94.62 | 462.8 | 94.03 | 731.1 |
| 99.22 | 201.0 | 98.60 | 251.9 | 95.42 | 252.1 | 95.15 | 496.5 | | |
| 99.35 | 289.3 | 98.84 | 329.3 | 95.97 | 276.8 | 95.56 | 542.3 | | |
| 99.46 | 391.6 | 99.03 | 436.2 | 96.58 | 314.6 | 95.83 | 574.7 | | |
| 99.50 | 497.4 | 99.14 | 540.6 | 97.12 | 372.8 | 96.27 | 648.0 | | |
| 99.56 | 606.1 | 99.26 | 644.8 | 97.63 | 464.8 | 96.57 | 718.1 | | |
| 99.62 | 745.7 | 99.29 | 732.4 | 97.98 | 571.9 | | | | |
| | | | | 98.21 | 677.9 | | | | |
| | | | | 98.32 | 747.7 | | | | |

TABLE 2. Miscibility Gap Data for the System Li-LiD and D/H Isotope Effect

| Temperature °C | Plateau Pressure[a] (Torr) | Misc. Gap Limits (mol % LiD) | | Isotope Effect, $P_{D_2}/P_{H_2}$ | | |
|---|---|---|---|---|---|---|
| | | Lower | Upper | $N_2 \sim 0$[b] | Plateau[c] | $N_2 \sim 1$[d] |
| 705 | 49.1 | 22.8 | 98.0 | 1.60 | 1.40 | 1.62 |
| 756 | 115.9 | 28.0 | 97.2 | 1.51 | 1.38 | 1.29 |
| 805 | 244.9 | 33.2 | 95.3 | 1.44 | 1.37 | 1.06 |
| 840 | 401.4 | 37.7 | 93.1 | 1.39 | 1.36 | 0.93 |
| 871 | 606.2 | 41.1 | 90.5 | 1.35 | 1.35 | 0.83 |

[a] Pressures calculated from Eq. 3

[b] $\ln(P_{D_2}/P_{H_2}) = -0.652 + 1096\ T^{-1}$

[c] $\ln(P_{D_2}/P_{H_2}) = 0.085 + 246\ T^{-1}$

[d] $\ln(P_{D_2}/P_{H_2}) = -4.100 + 4480\ T^{-1}$

$N_2$ = mole fraction LiH or LiD

TABLE 3. Plateau Pressures for the System Li-LiD

| Below Monotectic | | Above Monotectic | |
|---|---|---|---|
| Temperature (°C) | Pressure (Torr) | Temperature (°C) | Pressure (Torr) |
| 631.4 | 7.72 | 692.2 | 38.92 |
| 641.6 | 10.67 | 702.3 | 46.64 |
| 642.4 | 10.38 | 722.8 | 66.86 |
| 651.6 | 13.90 | 743.3 | 94.72 |
| 652.5 | 14.21 | 763.8 | 131.5 |
| 661.8 | 17.92 | 784.2 | 180.3 |
| 671.7 | 23.42 | 805.2 | 246.3 |
| 682.0 | 30.95 | 826.3 | 331.4 |
| | | 836.7 | 384.3 |
| | | 857.5 | 507.9 |
| | | 879.2 | 669.0 |

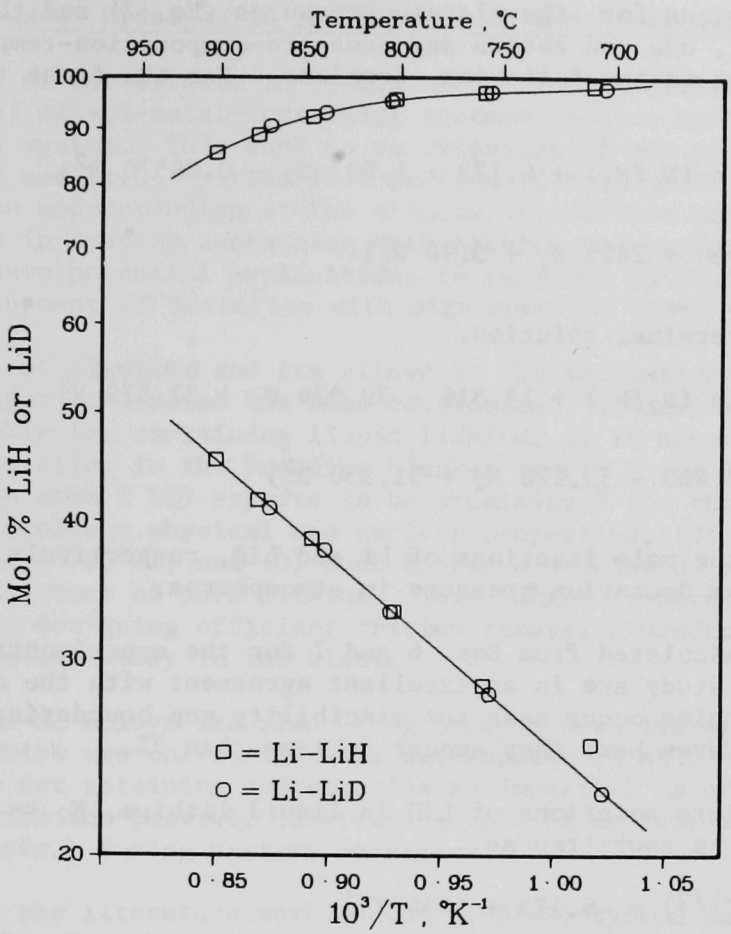


Fig. 7. Common Miscibility Gap Boundaries for the Systems Li-LiH and Li-LiD.

## 3. Calculated Properties

Reference 13 describes the details of the computational method used for the system Li-LiH to derive analytical expressions for the equilibrium constants, chemical potentials, activity coefficients, Sieverts' law constants, and other related properties. The same method was used for the present system. Briefly, for each homogeneous terminal solution, the data were fitted to an equation derived from the definition of the equilibrium constant and the Margules forms for the activity coefficients. The fitting was constrained by two conditions: (1) the same equilibrium constant must govern both terminal solutions and (2) the chemical activities of a component must be the same on both sides of the miscibility gap.

The equilibrium constant, K, for the reaction $1/2\ D_2(g) + Li(soln) \rightleftarrows LiD(soln)$ was then calculated to give

$$\ln K\ (atm^{-1/2}) = -6.647 + 8013\ T^{-1} \qquad (5)$$

From the expressions for the plateau pressures (Eq. 3) and the equilibrium constant (Eq. 5), one can obtain any pressure-composition-temperature relationship according to the following equations. For the first terminal solution,

$$\ln \sqrt{P_{D_2}} = \ln (N_2/N_1) + 6.172 + 1.007\ N_2 - 0.08570\ N_2^2 \qquad (6)$$
$$- (1/T)\ (5634 + 2626\ N_2 + 3198\ N_2^2)$$

and, for the second terminal solution,

$$\ln \sqrt{P_{D_2}} = \ln (N_2/N_1) + 15.316 - 39.924\ N_2 + 33.879\ N_2^2 \qquad (7)$$
$$- (1/T)\ (18{,}463 - 55{,}120\ N_2 + 51{,}330\ N_2^2)$$

where $N_1$ and $N_2$ are the mole fractions of Li and LiD, respectively, and $P_{D_2}$ is the equilibrium deuterium pressure in atmospheres.

The isotherms calculated from Eqs. 6 and 7 for the experimental temperatures of this study are in an excellent agreement with the data points. The largest discrepancies occur near the miscibility gap boundaries of the 871°C isotherms, but even here they amount to less than 3%.

For the very dilute solutions of LiD in liquid lithium, $N_2 << 1$, $N_1 \sim 1$, and Eq. 6 may be rewritten as

$$\ln K' \ (\text{atm}^{-1/2}) = -6.172 + 5634\ T^{-1} \qquad (8)$$

where $K' \left(= N_2/\sqrt{P_{D_2}}\right)$ is the Sieverts' constant. Very dilute solutions of hydrogen isotopes in liquid lithium are of particular interest in fusion reactor applications.

4. D/H Isotope Effect

Comparison of data between the Li-LiH and Li-LiD systems allows one to make estimates of the D/H isotope effect by calculating the $P_{D_2}/P_{H_2}$ ratios as functions of temperature and concentration. Due to the scatter in the data, the analytical functions derived for $P_{H_2}$ and $P_{D_2}$ shows errors sufficiently large to preclude calculation of accurate $P_{D_2}/P_{H_2}$ ratios in the concentration ranges of homogeneous solutions. The isotope effect was, therefore, evaluated only for the plateau region and for the extreme compositions of the phase diagram, $N_2 \sim 0$ and $N_2 \sim 1$.

The results are shown in columns 5, 6, and 7 of Table 2. In the plateau region, the temperature coefficients are almost negligible and, since the miscibility gap boundaries are identical for the two systems, the isotope effect appears to reside principally in the gas phase.

C. Solutions of Hydrogen in the β-Phase of the Li-Al System (E. Veleckis)

As part of our efforts to determine the fundamental thermodynamic properties of alkali-metal-containing systems we have initiated a study of the Li-Al-$H_2$ system. This work is an extension of our previous investigations of the Li-$H_2$ and Li-$D_2$ systems (see Section II B and Ref. 13) and is aimed at developing an understanding of the effects of additive metals on the activity coefficients in systems containing both lithium and hydrogen. The resultant data could have potential applications to research on fusion reactors[14] and to the development of batteries with high specific power and energy.[15]

The use of aluminum and its alloys as low-activation materials for fusion reactor blanket structures has been considered.[14] Since such structures would not be suitable for containing liquid lithium, it is necessary to employ a solid lithium alloy in the breeding blanket itself. The β-phase of the Li-Al system (48-56 atom % Li) appears to be promising[14] for that purpose because it has (1) excellent physical and nuclear properties, (2) sufficiently high melting point (∿700°C), and (3) much higher dissociation pressures of hydrogen isotopes than those of pure lithium. This latter property is especially important for designing efficient tritium removal procedures and for maintaining a low tritium inventory in the blanket.

Solid Li-Al alloys are also being used as negative electrodes in Li/S batteries, which are currently under development at ANL.[15] The capacity of these alloys for retaining hydrogen (as an impurity) is of interest in connection with the possible interfering role of ambient impurities (*e.g.*, H, O, N, C, *etc.*) during battery operation.

Most of the literature work on the Li-Al-$H_2$ system has been limited to studies of the thermal decomposition of $LiAlH_4$. This decomposition is known[16,17] to occur in at least three stages: (1) an exothermic reaction in the range 187-218°C evolving ∿50% of the total hydrogen, (2) an endothermic reaction from 228-282°C evolving an additional ∿25% $H_2$, and (3) a final endothermic reaction between 370 and 480°C evolving ∿ 22% $H_2$. According to the most recent thermal decomposition study,[18] the losses of hydrogen in these three stages correspond respectively to the formation of the following compounds: (1) $LiAlH_2$, (2) LiAlH, and (3) a homogeneous solution of hydrogen in a Li-Al alloy of unknown composition. Recently, Wiswall and Wirsing[19] have investigated tritium extraction rates from a powdered alloy between 400 and 600°C.

A study was initiated to investigate the direct interaction between hydrogen and the β-phase by measuring the dissociation pressure of hydrogen over solid solutions of hydrogen in the β-phase as a function of temperature, hydrogen concentration, and alloy composition. The equipment and the procedures being used in this study are essentially identical to those previously described for the Li-LiH system.[13]

Approximately 1.5 g of powdered β-phase alloy (52.9 at. % Li) was sealed *in vacuo* in an iron capsule having sufficiently thin (0.015-in.) walls to allow rapid diffusion of hydrogen. The capsule was placed in the Sieverts' apparatus and heated to the desired temperature. Hydrogen was added to the sample in small, measured portions, and the equilibrium pressure was recorded after each addition.

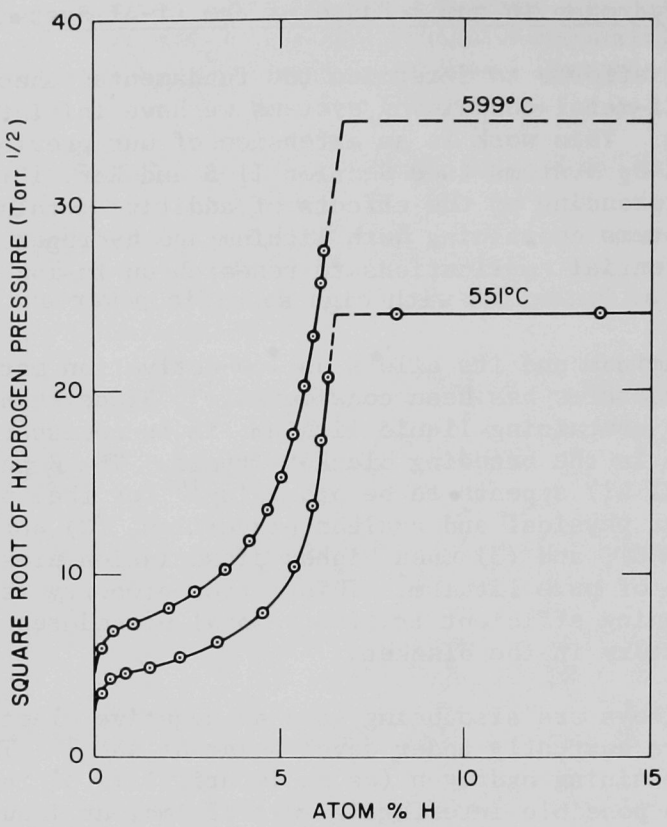


Fig. 8. Decomposition Pressure of Hydrogen in the β-Phase of the Li-Al System

To date, isotherms have been determined at 551 and 599°C. They are shown in Fig. 8, where the square root of hydrogen pressure is plotted against at. % H. In the range 0-6 at. % H, hydrogen pressure increases monotonically with concentration, an indication of a homogeneous condensed phase. The shapes of the isotherms, however, suggest the possibility of a miscibility gap existing at lower temperature. At ∿6 at. % H, the isotherms become flat, indicating the beginning of a wide miscibility gap of which the upper boundary presumably corresponds to LiAlH (33.3 at. % H).

After the completion of the second isotherm (at 551°C) the alloy contained 15.9 at. % H, which is well within the miscibility gap. This material was used to determine hydrogen plateau pressures as a function of temperature The results are shown in Table 4. The fluctuations in the hydrogen concentration shown in the table have resulted from (1) changes in hydrogen content of the residual volume at different temperatures, and (2) additions or subtractions of small amounts of hydrogen in order to accelerate equilibration of the system. The plateau pressures, P, in Table 4 may be represented by

$$\ln P \text{ (Torr)} = 20.46 - 11{,}597\ T^{-1}$$

with a correlation coefficient of -0.99989 for the regression. It is of interest to note that our plateau pressures agree well with those reported[18] for the third stage in the thermal decomposition of $LiAlH_4$, thus confirming the presence of similar condensed phases in both experimental approaches.

TABLE 4. Equilibrium Hydrogen Pressures over Two-Phase Mixtures of the System $\beta(LiAl)-H_2$

| Temperature (°C) | Hydrogen Pressure (Torr) | Concentration (at. % H) |
|---|---|---|
| 424 | 45.4 | 17.3 |
| 443 | 71.4 | 21.4 |
| 465 | 117.0 | 20.1 |
| 492 | 201.0 | 18.5 |
| 514 | 311.8 | 23.7 |
| 528 | 403.1 | 19.1 |
| 551 | 582.5 | 15.9 |

Further work on the system will be directed toward (1) a more detailed delineration of the dilute region, (2) determination of temperature coefficients, and (3) effects of changes on the alloy composition (within the limits of the β-phase).

D. Studies of the Solubility of $Li_3N$ in Liquid Lithium and the Thermal Decomposition of $Li_3N$ (R. M. Yonco and E. Veleckis)

In previous reports,[10,20] we discussed the shortcomings of published physicochemical data on the Li-N, Li-O, and Li-C binary systems. As part of a comprehensive program to measure the thermodynamic properties and phase relationships in these systems, the solubility of $Li_3N$ in lithium and the thermal decomposition of $Li_3N$ have been studied. Thus far, the program has produced new values for the solubility of $Li_3N$ in lithium[11] and, in the last period, the melting point of $Li_3N$ and the equilibrium pressure values for the thermal decomposition of solid $Li_3N$. These data have permitted the calculation of (1) the Sieverts' law constant for dilute solutions of nitrogen in lithium and (2) estimated values for the standard free energy of formation of solid $Li_3N$. Details of the experimental procedures and the treatment of the data are given below.

The apparatus previously used to measure the solubility of $Li_3N$ in liquid lithium was modified for the decomposition pressure measurements by the addition of (1) an Armco iron vessel to contain the solid $Li_3N$ sample (as shown in Fig. 9) and (2) a gas-sampling manifold which consisted of three pressure gauges (a 0-1 Torr capacitance manometer and 0-20 and 0-100 Torr calibrated aneroid gauges) and a gas-sampling port. The stirred pool of lithium served as an isothermal environment for the $Li_3N$ container.

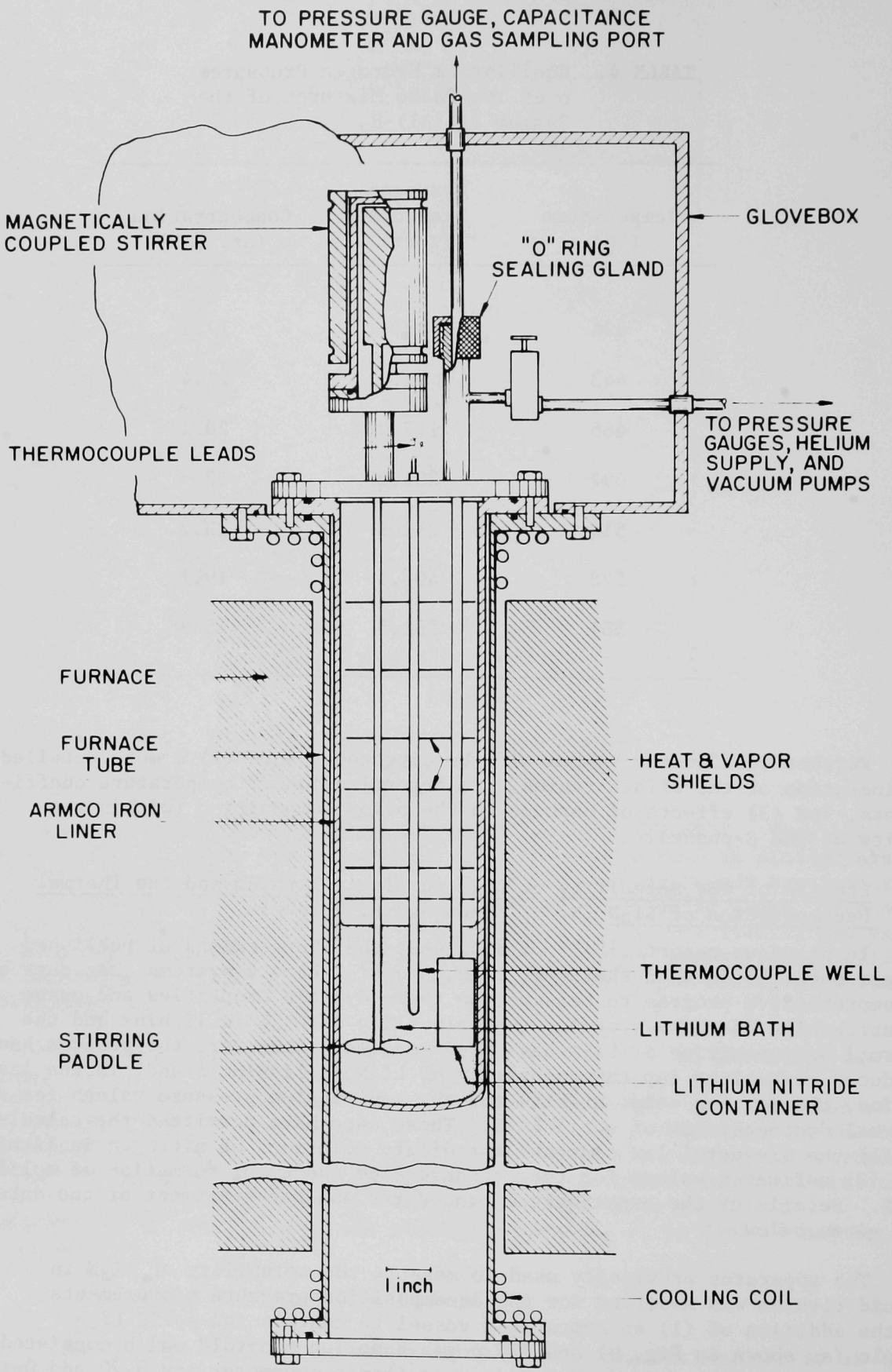


Fig. 9. Apparatus for Measuring the Decomposition Pressure of $Li_3N$

Decomposition pressure measurements were made in the following manner. The iron container was filled with 8.75 gm (0.25 mole) of granular $Li_3N$. The vessel was heated to a desired temperature, rapidly pumped out, and then isolated from the pump. The nitrogen gas evolved from the decomposition of $Li_3N$ was allowed to expand into the evacuated manifold. When equilibrium was achieved (as evidenced by a stable pressure reading), the nitrogen pressure was measured and a sample of the gas phase was taken for mass spectrometric analysis. A total of eight pressure measurements, made at temperatures ranging from 660° to 778°C, are listed in column 2 of Table 5. The nitrogen assay of the gas samples was consistently >99%, the major impurity being helium. The amount of nitrogen removed from the system for each gas analysis was negligibly small and had no effect on the values of subsequent pressure measurements.

The same apparatus was also used to measure the melting point of pure $Li_3N$. Fresh $Li_3N$ was charged into the iron container, the lithium bath was removed, and a stainless steel clad thermocouple was inserted into the container. The container was pressurized with nitrogen to 1200 Torr to suppress the loss of nitrogen from the compound and the melting point was determined from the thermal halts in a single melt-freeze cycle of the $Li_3N$. The measured melting point of 813 ± 1°C is in good agreement with the published value of 815°C.[21]

TABLE 5. Decomposition Pressures of Solid $Li_3N$, Solubilities and Activity Coefficients at the Liquidus Line, Equilibrium Constants, and Sieverts' Constants for the Li-$Li_3N$ System[a]

| Temp. (°C) | $P'$[b] (Torr) | $N'_{Li_3N}$[c] | $\gamma'_{Li}$ | $K$ ($atm^{-1/2}$) | $K_s$[d] |
|---|---|---|---|---|---|
| 660.6 | 0.239 | 0.120 | 1.025 | 76.8 | 6.29 |
| 681.2 | 0.648 | 0.139 | 1.032 | 48.8 | 4.42 |
| 701.4 | 1.79 | 0.169 | 1.047 | 31.3 | 3.20 |
| 720.2 | 4.23 | 0.195 | 1.062 | 21.4 | 2.38 |
| 739.2 | 9.90 | 0.236 | 1.091 | 15.1 | 1.86 |
| 758.3 | 24.8 | 0.285 | 1.132 | 10.4 | 1.40 |
| 772.3 | 53.0 | 0.360 | 1.216 | 8.03 | 1.18 |
| 777.8 | 68.1 | 0.380 | 1.242 | 7.32 | 1.10 |

[a] These data were collected randomly with respect to temperature, not sequentially as listed.

[b] Primed symbols represent solutions that are saturated with respect to $Li_3N$.

[c] Values interpolated from Fig. 4 of Ref. 11.

[d] Sieverts' constant, $K_s = N_{Li_3N}/\sqrt{P}$, in units of mole fraction per $atm^{1/2}$.

The thermal decomposition pressures in conjunction with $Li_3N$ solubility values (taken from Fig. 4, Ref. 11) allow the calculation of the thermodynamic properties of the Li-$Li_3N$ system. The reaction of gaseous nitrogen with liquid lithium may be written as

$$1/2\ N_2(g) + 3\ Li(soln) \rightleftarrows Li_3N\ (soln) \tag{9}$$

The equilibrium constant, K, for reaction (9) is given by

$$K = \frac{N_2\gamma_2}{N_1^3\gamma_1^3\sqrt{P}} \tag{10}$$

where $N_1$ and $N_2$ are the mole fractions of lithium and $Li_3N$, respectively, $\gamma_1$ and $\gamma_2$ are their activity coefficients, and P is the nitrogen pressure.

The calculation of K requires experimental values for $N_2$ and P (available for saturated solutions only) and values for $\gamma_1$ and $\gamma_2$. A reasonable estimate of the $\gamma$'s can be made from the Margules[22] equations that are truncated at the quadratic term. For the solvent lithium, this would give

$$\ln \gamma_1 = \frac{\alpha}{RT} N_2^2 \tag{11}$$

where $\alpha$ is a temperature-independent constant. By application of the Gibbs-Duhem equation to Eq. 11, one obtains for the activity coefficient of the solute $Li_3N$

$$\ln \gamma_2 = \frac{\alpha}{RT} (N_1^2 - N_1'^2) - \ln N_2' \tag{12}$$

where the primed symbols represent values at the liquidus boundary. The constant, $\alpha$, was evaluated by substituting Eq. 11 into Eq. 10, selecting values of P and $N_2$ existing at the liquidus boundary, defining solid $Li_3N$ as the standard state (*i.e.*, $N_2'\gamma_2' = 1$), and choosing a value for $\alpha$ ($\alpha$ = 3.14 kcal/mole) such that a plot of ln K *vs.* 1/T would give a statistically best straight line.

The resulting equations for the equilibrium constant and the standard free energy of formation, $\Delta G_f^\circ$, of solid $Li_3N$ are given by Eqs. 13 and 14.

$$\ln K\ (atm^{-1/2}) = -16.73 + 19{,}670\ T^{-1} \tag{13}$$

$$\Delta G_f^\circ (kcal/mol) = 33.2 \times 10^{-3}\ T - 39.1 \tag{14}$$

At 1000°K, Eq. 14 would give $\Delta G_f^\circ$ = -5.9 kcal/mol, which is significantly different from the value of -9.46 kcal/mol listed in the JANAF Tables.[23]

On the other hand, our values for the standard enthalpy ($\Delta H_f^\circ$ = -39.1 kcal/mol) and entropy ($\Delta S_f^\circ$ = -33.2 e.u.) are in very good agreement with extrapolations to 1000°K of recent low temperature calorimetric work at ANL where $\Delta H_f^\circ$ = -40.01 kcal/mol[24] and $\Delta S_f^\circ$ = -32.55 e.u.[25] are reported. The good agreement with the ANL calorimetric values lends support to the thermodynamic values resulting from our work.

Dilute solutions of $Li_3N$ and the Sieverts' law constant, $K_s$, are of particular importance to the controlled thermonuclear research program.

At infinite dilution, Eq. 11 may be rewritten to give the expression for $K_s$

$$\lim_{N_2 \to 0} \frac{N_2}{\sqrt{P}} = K_s = \frac{K}{\gamma_2^*} \tag{15}$$

where $\gamma_2^*$ is the activity coefficient of $Li_3N$ at infinite dilution. The numerical value of $\gamma_2^*$ is derived by applying the condition $N_1 \to 1$ to Eq. 12. Table 5 lists the thermodynamic properties that were calculated and the experimental points from which they were derived. The Sieverts' constant in Table 5 can be represented by the linear equation.

$$\ln K_s(\text{atm}^{-1/2}) = -13.80 + 14{,}590\ T^{-1} \tag{16}$$

with a correlation coefficient of 0.99980.

The experimental effort in this program is now directed to the measurement of the solubility of oxygen in liquid lithium. The solubility apparatus has been modified and sampling and analytical procedures are being established.

# III. TRITIUM CONTAINMENT AND CONTROL TECHNOLOGY FOR FUSION REACTORS

The work described in this section is being carried out in support of the controlled thermonuclear research program and is intended to contribute to the development of (1) an extended materials and process data base and (2) a more detailed understanding of the operating characteristics and performance criteria for the tritium-handling systems of fusion power reactors.

## A. Experimental Studies of Tritium Barrier Concepts for Fusion Reactors

(E. H. Van Deventer, R. H. Pelto* and V. A. Maroni)

### 1. Hydrogen Permeation Characteristics of Multiplex Metal Structures

A program is in progress to evaluate the potential utility of multilayered metal composites as barriers to tritium migration in fusion devices and reactors. The motivation for this research program has been discussed in a previous publication.[26] The objective of the program is to prepare and characterize multilayered laminates in which a material with a relatively low hydrogen permeability (*e.g.*, selected copper alloys, beryllium alloys, and aluminum) is sandwiched between layers of the kinds of structural metals currently considered to have application in fusion technology (*e.g.*, refractory metal alloys and stainless steels). These multilayered materials are expected to be useful in the construction of (1) steam-generator tubing and other heat-transfer/energy conversion system components, (2) liners for the blanket-shield interface, and (3) ductwork and other hardware for the transport, processing, and storage of tritium. An added advantage of the use of composite or multiplex materials is that compatibility problems associated with the interfacing of blanket, primary coolant, and secondary working fluids can be ameliorated by selecting (for the exterior layers of the multiplex) metals that are compatible with the fluid being contacted. (For example, a liquid lithium circuit could be interfaced with a high-pressure helium loop as follows: lithium to Nb-1%Zr/304-SS to helium.)

Hydrogen permeation data have been collected in our laboratory for the following metallurgically bonded composites:** 316-SS(0.5mm)/Cu(1.0mm)/316-SS(0.5mm), Nb(0.27mm)/304-SS(0.25mm), and Nb(0.19mm)/Cu(0.42mm)/304-SS(0.25mm). Permeation data and least-squares-refined permeation curves for these composite materials and for 316- and 304-SS are plotted in Figs. 10 and 11. In addition to the experimentally determined permeation curves, Figs. 10 and 11 contain calculated permeation curves for the 316-SS/Cu/316-SS composite and the Nb/Cu/304-SS composite, respectively. These calculated curves were derived using a model which assumes that the layers of a multiplex may be treated as a series of resistors to hydrogen flow and that Fick's law for diffusion is obeyed. Based on these assumptions, the calculated hydrogen permeation coefficient, $K_t$, of a multiplex with N layers is given by

$$K_t = \left(\sum_i^N X_i/K_i\right)^{-1} \qquad (17)$$

---

*1975 Spring Undergraduate Research Program Participant from Michigan State University.

**The numbers in parentheses give the thicknesses of the individual layer materials. All three composites were fabricated by Texas Instruments Co., Attleboro, Mass.

where $K_i$ is the permeation coefficient for the $i^{th}$ layer material, and $X_i$ is the thickness of the $i^{th}$ layer.

Values for the permeation coefficient of niobium, $K_{Nb}$, versus temperature were determined by solving Eq. 17 for $K_{Nb}$ in terms of (1) $K_{304\text{-SS}}$ (from Fig. 11), (2) permeability values for the Nb/304-SS composite, and (3) the measured thicknesses of Nb and 304-SS in the latter composite. These values of $K_{Nb}$, together with values of $K_{304\text{-SS}}$, $K_{Cu}$ (from Section III.A.2.), and the measured layer thicknesses of the Nb/Cu/304-SS composite were inserted in Eq. 17 to obtain the calculated curve for the Nb/Cu/304-SS composite shown in Fig. 11.

In the analysis of differences between measured and calculated permeation curves, effects due to interactions at the two surfaces exposed to hydrogen (upstream and downstream) are assumed to cancel. It is important to note that this assumption will only be valid if the oxidizing potentials due to impurities in the upstream and downstream hydrogen environments are identical in all correlated experiments. Taking this to be the case, the observed differences between predicted and measured permeabilities are considered to be a consequence of either alloying or impurity interactions at the metallurgical interfaces. In the case of the 316-SS/Cu/316-SS composite, the observed permeation rate is lower than the calculated rate over the entire temperature range investigated (Fig. 10). It is possible that interactions at the Cu/316-SS interface create an added resistance to hydrogen migration. The least-squares-refined permeation curve for the Nb/Cu/304-SS composite gives slightly higher permeation rates than does the calculated curve for this composite obtained by the somewhat circuitous route described above. Because of the complexity of the intermetallic interactions involved and the sensitivity of the hydrogen permeability of niobium to oxidizing potentials,[27] we refrain from any further speculation about subtle differences between calculated and experimental values for the niobium-containing composites at this time.

As a general rule, the integrity of metallurgically bonded composites examined thus far was found to be unaffected by large-scale hydrogen throughput. Electron microprobe examinations of each composite before and after hydrogen permeation experiments showed no evidence of element redistribution across the interfaces due to passage of hydrogen. The amount of hydrogen that permeated through each composite was in excess of 8cc(STP)/cm$^2$. In conventional fusion reactor stream generator systems where the partial pressures of various hydrogen isotopomers (*e.g.*, $H_2$, HT, $T_2$) are expected to be many orders of magnitude lower than those used in our experiments, the passage (by permeation) of 8 cc(STP)/cm$^2$ of hydrogen through the steam generator tube walls would probably require upwards of 100 years of continuous operation.

## 2. Development of Barrier Layer Materials for Multiplex Metal Structures

The preceding section (III.A.1.) contained a summary of the potential applicability of multiplex metal composites as barriers to tritium migration (by permeation) through fusion reactor construction materials that are subject to operation at elevated temperature (>300°C). In this section, we discuss the results of experimental studies to identify and characterize materials that would be suitable for use as the barrier layer in stainless steel-clad

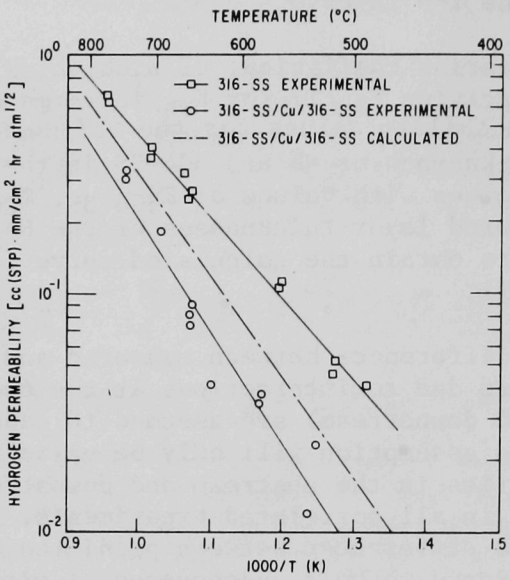


Fig. 10. Hydrogen Permeability *vs.* Reciprocal Kelvin Temperature for 316-SS and the 316-SS/Cu/316-SS Composite Together with the Calculated Permeation Curve for the 316-SS/Cu/316-SS Composite

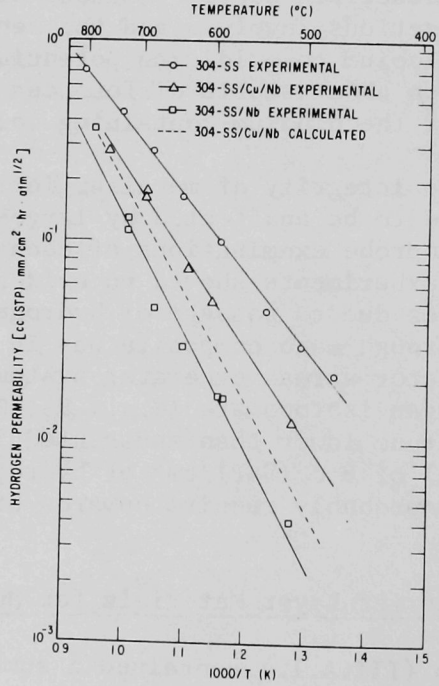


Fig. 11. Hydrogen Permeability *vs.* Reciprocal Kelvin Temperature for 304-SS, the 304-SS/Nb Composite, and the 304-SS/Cu/Nb Composite Together with the Calculated Permeation Curve for the 304-SS/Cu/Nb Composite

multiplexes. Initial studies have focused on copper and its alloys because (1) their relevant physical and mechanical properties (particularly thermal expansion coefficients) are well matched with those of stainless steels insofar as composite preparation and high-temperature integrity are concerned, and (2) a substantial industrial technology base for the preparation of both metallurgically and mechanically bonded copper/stainless steel composites appears to exist.

Hydrogen permeation measurements were made on pure copper and on a copper-base alloy (Cu-10 wt % Al-4 wt % Fe). A detailed description of the equipment and procedures used in these studies and in the studies described in Section III.A.1. will be presented in a future publication.[28] Briefly, the measurements were made on 1- to 2-mm-thick circular membranes with surface areas of $\sim 4$ cm$^2$. Each membrane was electron-beam welded between two stainless steel couplings in such a way that it provided a sealed wall between the compartments formed by the two couplings. One compartment was connected to a constant pressure hydrogen supply; the other compartment was connected to a Toepler pump. Measurements of the permeation rate through a membrane were made by determining the quantity of gas collected by the Toepler pump over known time intervals. The upstream hydrogen pressures used were in the range from 50 to 600 Torr.

The permeability of pure copper was found to be roughly proportional to the half-power of the upstream hydrogen pressure over the temperature and hydrogen pressure ranges examined in our work. (The pressure dependence of the permeability for the copper-aluminum-iron alloy remains to be studied.) The hydrogen permeation data obtained for pure copper and the copper-aluminum-iron alloy are shown in Fig. 12 together with least-squares refined permeation curves (solid lines). Also shown in Fig. 12 are the permeability curves for these same materials obtained by other investigators.[29-32] In the case of pure copper, the agreement with the results of Belyakov and Zvezdin[32] and Perkins and Begeal[29] is very good. The work of Smithells and Ransley[31] dates back to 1935, and the apparent discrepancy may be a reflection of the purity of the samples used in their studies. The curve representing the results of Ehrmann *et al.*[30] was extrapolated from the temperature region of their data (170 to 240°C). Also, there was some uncertainty in the conversion of the permeability units used by Ehrmann *et al.* to the units that we normally use. In the case of the copper-aluminum-iron alloy, there is a sizable disparity between our data and the data of Belyakov and Zvezdin.[32] We are of the opinion that the reduced permeability of this alloy (compared to the permeability of pure copper) is due to formation of an extremely stable, bimetallic, surface-impurity coating on the alloy's surface. If this is indeed the case, and if the extent of formation of this coating is dependent on impurity potentials in the environment surrounding the alloy prior to or during permeation measurements, then the disparity between our work and that of Belyakov and Zvezdin[32] may be attributable to differences in background impurity levels and/or prior sample history. However, it should also be noted that the permeation rates measured in our study of this alloy are near the background levels of our gas collection apparatus (Toepler pump), which may have biased our readings in the direction of being too high. In order to circumvent this problem in future work, we have constructed an all-metal, high vacuum, hydrogen permeation apparatus which will provide greater sensitivity at low hydrogen permeation rates.

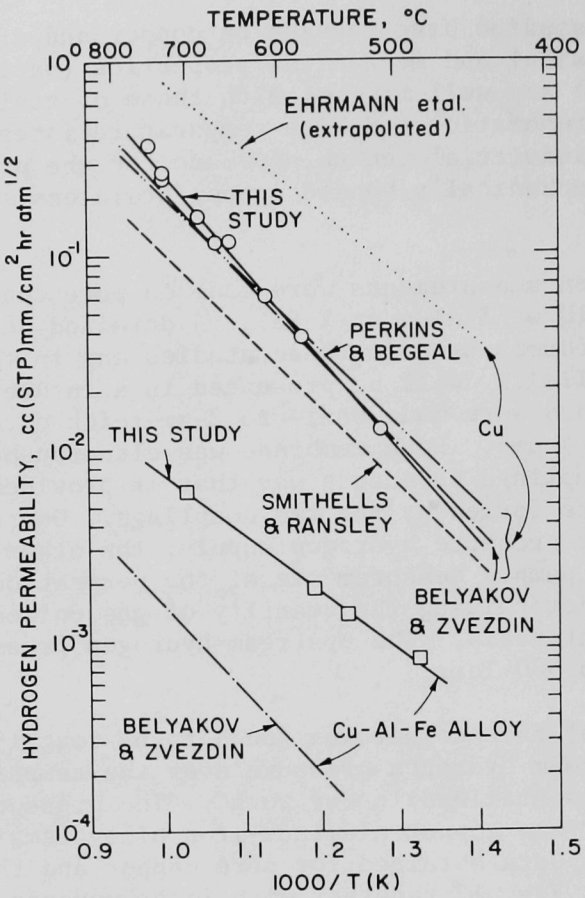


Fig. 12. Hydrogen Permeation Data and Least-Squares-Refined Permeation Curves for Pure Copper and Cu-10 wt % Al-4 % Fe Alloy

Because the hydrogen permeability of pure copper is only a factor of from 2 to 5 lower than that of most conventional stainless steels (see Figs. 10 and 11) at elevated temperatures (>400°C), its potential value as a tritium-barrier layer in stainless steel-clad composites is low. However, the copper-aluminum-iron alloy would be very attractive for use as a barrier layer, if its permeability can be kept at least as low as our results in Fig. 12 indicate. For example, at 600°C, the hydrogen permeability of a 304-SS/Cu-Al-Fe alloy/304-SS composite (with all three layers having the same thickness) would be ∿50 times lower than the permeability of an equally thick layer of 304-SS (based on our data for the copper-aluminum-iron alloy and for 304-SS).

Work is currently in progress to prepare a series of metallurgically bonded 304-SS/Cu-Al-Fe alloy/304-SS composites in which the 304-SS and Cu-Al-Fe alloy are subjected to a variety of surface pretreatments prior to bonding. The hydrogen permeation characteristics of these composites will then be examined.

### 3. Fabrication Efforts on Multiplex Materials

During the past year, an effort has been undertaken to investigate the prospects for preparing multiplex metal laminates in seamless tube form and joining sections of these laminates by various welding procedures. The ANL Materials Science Division prepared a mechanically bonded 304-SS/Cu/304-SS composite in seamless tube form by drawing concentric cylindrical tubes of 304-SS and copper into intimate contact with one another. Sections of this composite tubing were then joined contiguously (layer to corresponding layer) to form a linear joint as shown in Fig. 13. The joint was fabricated by sequentially electron-beam welding (with controlled penetration) all the seams formed by (1) the interior 304-SS layer, (2) the copper half-cylindrical inserts, and (3) the outer 304-SS half-cylindrical inserts. In actual operation, this linear joint could be given additional support by surrounding the weld region with a cylindrical 304-SS collar. X-rays of the entire welded zone showed no evidence of weld imperfection.

Tests of the integrity of the linear joint followed by sectioning to determine the weld penetration depths are planned. Future work will also include an attempt to contiguously T-weld two sections of composite seamless tubing.

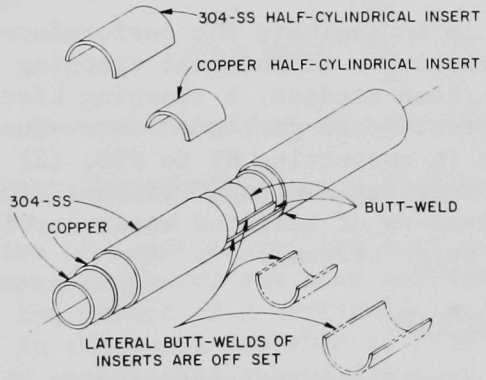


Fig. 13. Contiguous Butt-Weld of a 304-SS/Copper/304-SS Metal Composite Tube

### B. Tritium Trapping Kinetics in Inert Gas Streams (R. H. Pelto*, C. J. Wierdak**, and V. A. Maroni)

This effort is directed toward studies of the kinetics of chemical trapping reactions involving tritium in inert gas streams (e.g., helium, argon, nitrogen). Specific gas stream environments that have practical applications in fusion devices and reactors include (1) high-pressure helium streams used as coolant

*ANL Undergraduate Research Program Participant from Michigan State University.

**ANL Undergraduate Research Program Participant from Illinois Institute of Technology.

circuits for power reactor blankets, (2) low-pressure inert gas streams used in conjunction with either double containment jackets for isolated reactor components or whole-room atmosphere purges, and (3) the mainstream fuel cycle for D-T fueled devices or reactors. With regard to the behavior of tritium in helium coolant circuits and in inert gas purge streams, significant advantage in terms of overall tritium containment can be gained[33] by converting the tritium present in these streams to $T_2O$ or HTO and then sorbing, desiccating, or otherwise fixing the $T_2O$ or HTO in a medium that is suitable for (1) tritium regeneration and reinsertion into the mainstream fuel cycle or (2) consolidation of low-level tritiated wastes in preparation for long-term burial.

The chemical trapping requirements imposed by the needs of the mainstream fuel purification and recycle system of a D-T fueled fusion reactor are substantially different from those of the gaseous coolant and purge circuits. During the course of passage through the plasma chamber, the D-T fuel mixture will invariably pick up low levels of nonmetallic impurities (*e.g.*, O, N, and C). Since only a small fraction (<5%) of the injected fuel actually undergoes fusion in a single burn cycle, it is essential (for power reactors) to continuously recycle the unburned D-T mixture. Because of the deleterious effects of impurities on plasma energy balance and stability, the impurities picked up during one burn cycle must be removed prior to reinjection of the recycled fuel mixture. It would be desirable to identify chemical trapping media that can effectively remove these nonmetallic impurities without simultaneously tying up a large quantity of tritium.

Our present objective is to evaluate the performance of materials that might be suitable for the two types of chemical trapping operations summarized above. As a beginning for these studies, a trapping kinetics apparatus was assembled, and a series of tests were performed to evaluate (1) the efficiency of heated $CuO/MnO_2$ mixtures in converting HT to HTO, (2) the efficiency of heated magnesium beds in converting HTO to HT without simultaneously pumping the HT, and (3) the effectiveness of selected water-sorbing media in trapping HTO from flowing inert-gas purge streams.

## 1. Experimental Procedure

The apparatus developed for these studies is shown in Fig. 14. The upper branch is designed to permit series testing of an oxidizer bed (*e.g.*, $CuO/MnO_2$) and a reducer bed (*e.g.*, magnesium metal) with provision for by-passing of either or both beds. The lower branch is designed to permit testing of various water-sorbing or desiccating media and is also fitted with a by-pass. Tritium from the carrier-gas cylinder ($\sim$1.7 μCi/cc of HT in argon) is introduced to the pulse chamber with both solenoid valve B and backup valve C closed. Pulses of the tritiated carrier gas are delivered to the trapping circuit by closing valve A, opening valve C, and triggering solenoid valve B. (After triggering of a pulse, valve C is closed to guard against any low-level tritium leakage across the seat of solenoid valve B.) Solenoid valve B is controlled by an electronic pulser which opens the valve for a set length of time; hence, uniform-sized pulses of the tritiated carrier gas are delivered with each triggering. (This uniformity of pulse was demonstrated experimentally.) Tritium counting is performed with a Johnston Laboratories Model 955B Tritium Monitor.

The apparatus in Fig. 14 is set up for either once-through flow studies using an inert sweep gas (valve D open, valve E closed, and valve F open) or recycled-flow studies (valve D closed, valve E open, and valve F closed). Thus, both instantaneous and long-term performance of various conversion beds and water-trapping media can be investigated.

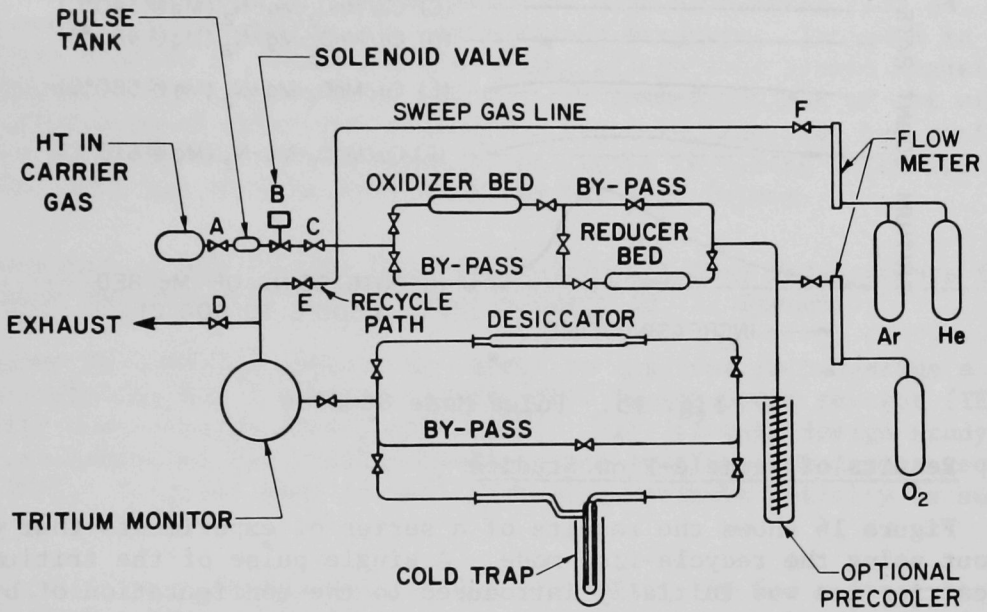


Fig. 14. Apparatus for Tritium Trapping Studies

2. Results of Once-through Pulse-flow Studies

In this series of experiments, the tritium pulses were swept once through a variety of conversion-bed and trap configurations and exhausted. This was done to test the effect of a particular bed and trap combination on tritium concentration in the sweep gas when tritium is admitted to the system in bursts. Preliminary experiments showed (1) that the tritium in the carrier gas is mostly in the form HT when it leaves the pulse chamber, (2) that the $CuO/MnO_2$ bed converts essentially all of the HT to HTO in a single pass, and (3) that a liquid nitrogen-cooled copper mesh trap effectively removes HTO from the sweep gas but does not remove HT. Figure 15 contains the results of a set of experiments designed to test the performance of magnesium metal as a reducing-bed material. All results were obtained at a sweep-gas flow rate of 2 LPM. [The following designations are used in Fig. 15: B = by-pass; Mg = magnesium metal bed; $CuO/MnO_2$ = copper oxide/manganese dioxide mixture (50 vol % CuO, 600°C); and $N_2$ = liquid-nitrogen-cooled copper-mesh trap.] Curves A and B give evidence that there is some tritium hold-up by the magnesium bed. Curves C through F illustrate the performance of the magnesium bed at various temperatures. The bed does not significantly reduce HTO to HT at 340 or 420°C. At 580 and 610°C there is some evidence of reduction of HTO to HT, but the performance is still only marginal. Curve G shows the extent of tritium outgassing from a helium-swept magnesium bed as the bed is heated from 300 to 600°C. This curve was obtained after a series of HT pulses had been put through the bed at 300°C.

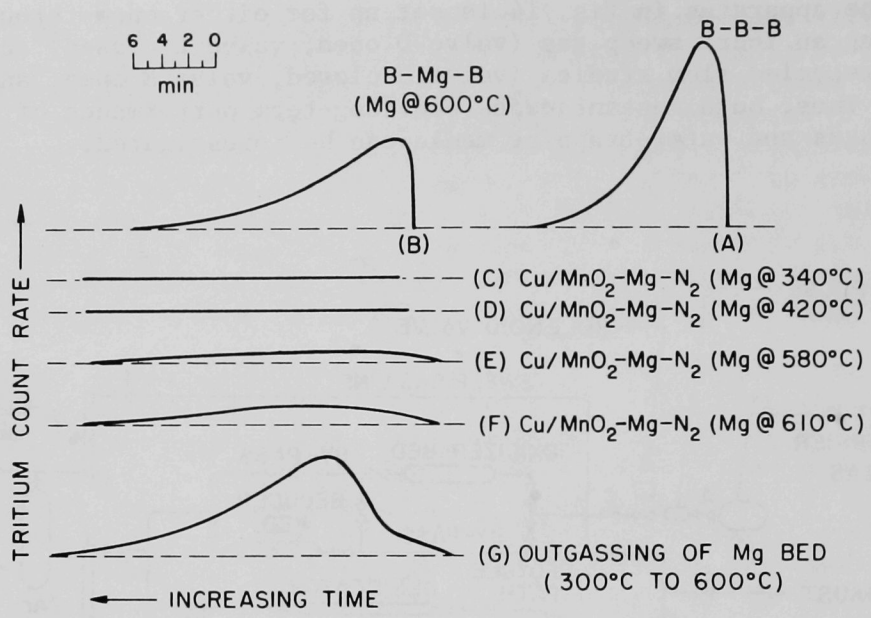


Fig. 15. Pulse Mode Studies

3. Results of Recycle-Flow Studies

Figure 16 shows the results of a series of experiments that was carried out using the recycle-flow mode. A single pulse of the tritium-containing carrier gas was initially introduced to the configuration of by-passes and converters listed at the right edge of the pulse and, thereafter, to other by-pass-converter-trap configurations as indicated. Results of the studies illustrated in Fig. 16 and of related studies can be interpreted as follows: (1) the tritium count rate in an all-by-pass configuration rapidly reaches a steady value (curve A), (2) the magnesium bed absorbs tritium at a slow but steady rate (curve B), (3) some permeation of tritium through the walls of the metal-bed containers cannot be ruled out, (4) there is no trapping of HT by the liquid nitrogen-cooled copper-mesh trap (configuration B-B-$N_2$ in curve

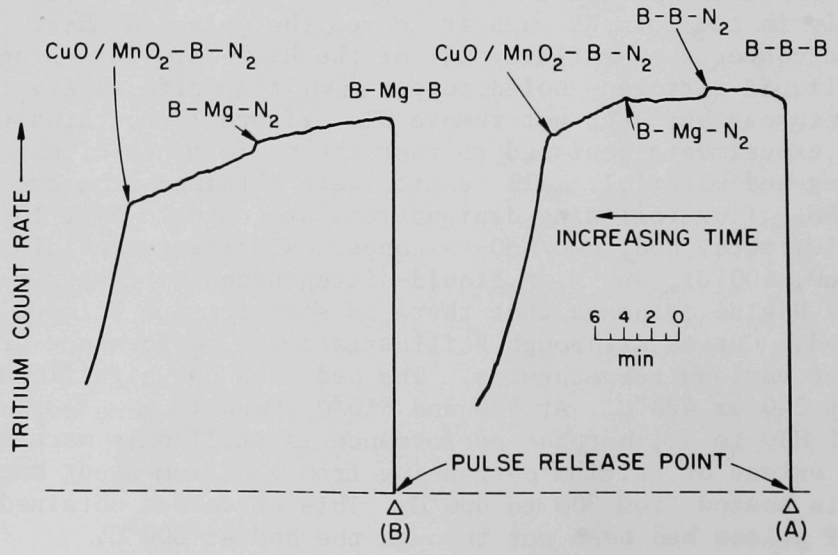


Fig. 16. Recycle Mode Studies

A; the discontinuity in the count rate when the nitrogen cold trap is inserted is due to a change in the overall system volume), and (5) the steeper slope for the B-Mg-$N_2$ configuration in curve B compared with the slope for the B-Mg-B configuration indicates that some back conversion of HT to HTO may occur as the HT leaves the magnesium bed.

4. Direction of Future Effort

Methods of improving the performance of magnesium-metal beds as reducing media for HTO pulses are currently in progress. Included in this work are (1) studies of magnesium-containing alloys that permit higher-temperature operation of the reducer bed and (2) investigations of the effects on bed performance of sweep-gas flow rate, particle size, and bed configuration. Efforts to characterize the kinetics of reactions involving tritiated hydrocarbons in inert gas streams will begin in the near future.

## C. Assessment of the Tritium Handling and Containment Requirements for a Tokamak Experimental Fusion Power Reactor (V. A. Maroni)

Argonne National Laboratory is currently involved in preparing a detailed design description for a tokamak experimental fusion power reactor (TEPR) to be built and operated during the 1980's. Part of this design study has been an assessment of the tritium-handling and tritium-containment requirements for the TEPR. Progress made to date in this assessment activity is summarized below:

The preliminary design point[34] for the TEPR calls for a first stage of operation (Stage I) in which (1) reactor level plasmas are tested and (2) sensible heat is produced in a optimally constructed stainless steel-$B_4C$ blanket. No provision for tritium breeding is included in Stage I. In a second stage of operation (Stage II) several of the Stage I blanket modules are replaced with a series of modified modules containing lithium in some form in order to test promising tritium breeding concepts.

It appears that operation of the TEPR at a cycle averaged power of $\sim$100 $MW_{th}$ will result in consumption (by burnup) of $\sim$16 g per day of tritium and $\sim$11 g per day of deuterium. Taking account of the fractional burnup and the extent to which a cold fuel gas-blanket is employed, we estimate that the gross fuel throughput could approach 2700 g per day (D+T). The cost of supplying tritium to the TEPR to offset the burnup may run from $5 to 15 million per year. The fueling costs associated with deuterium supply are negligible.

The tritium-handling facility for Stage I operation has been broken down into six major systems: fuel-delivery, fuel-circulation, fuel-processing, fuel-storage, in-plant-containment, and purge-processing. State II operation requires all six of these systems plus an additional system to provide blanket-processing. The principal features of these systems, as they are currently conceived, are outlined below. More detailed discussions of each system may be found in Ref. 34.

1. Fuel-Delivery System

The function of this system is vital to sustained operation of reactor-level plasmas in a TEPR. A substantial fraction of the total quantity of D-T fuel involved in a single burn cycle may have to be delivered to the plasma after initiation of the discharge. Fueling schemes that involve either high-speed injection of solid D-T pellets or application of a cold D-T gas blanket are leading candidates. Special features of each of these fueling schemes that are necessary to insure efficient recycle and adequate containment of tritium are being evaluated, and estimates of the additional costs associated with these special features are being made.

2. Fuel-Circulation System

The tritium-handling facility for the TEPR comprises a network of systems which either operate on or store the fuel at various stages of the fuel cycle. The subsystems and components that fall under the fuel-circulation system are those which provide the interfaces between the other six tritium-handling systems, *e.g.*, all interconnecting ductwork and piping, compressors, circulation pumps, the vacuum pumping equipment, numerous intermediate conditioning steps, monitoring equipment, the overall-facility control center, valves, by-passes, etc. Identification of the methodology for performing all of these diverse operations, evaulations of existing technology, and costing of the entire installaion are in progress.

3. Fuel-Processing System

This sytem consists of an integrated process involving a hot-getter/cryogenic-trap step (to remove non hydrogenous impurities) and a cryogenic-distillation step (to remove helium and protium). Alternatives to cryogenic distillation, including laser-excited isotope separation and multi-staged permeable membranes, will eventually come under study.

4. Fuel-Storage System

Various approaches to the provision of fail-safe fuel storage and storage access are being investigated. For the purposes of the present design study, consideration is given to a concrete barricaded vault containing three or more independently controlled storage cells. The cells house a temperature-sensitive hydrogen-gettering material, wherein uptake or release of tritium is controlled by temperature adjustments. The vault itself is provided with a quenching system that can rapidly remove thermal energy from the cells in the event of an incident that could compromise the storage of tritium. Also included in the assessment of this system will be those considerations that are pertinent to fail-safe transportation of tritium from a distant production facility. Prospects for near-term development of the required transportation and storage facilities based on existing technology appear to be excellent.

5. In-Plant-Containment System

Current thinking on this system suggests that consideration be given to three levels of tritium containment. Where it is possible to do so, construction of all components that come into direct contact with tritium should be made with low-permeability materials (*e.g.*, selected alloys, metal composites,

ceramic barriers), particularly in elevated temperature (>300°C) regions. It may be necessary to provide an external, closely fitted jacket with provision for in-jacket purging around those tritium facility components that (1) are susceptible to failure, (2) operate at elevated temperature, and/or (3) contain relatively large quantities of tritium. In addition, the main reactor hall and the other in-plant rooms that house tritium-handling systems will be designed to include hermetic sealing (from the environment) and an inert continuously processed atmosphere. The costs associated with these three levels of containment will be evaluated in parallel with the systems scoping and design activities.

6. Purge-Processing System

This system must be designed to remove tritium from both the jacketed and whole-room purge streams. Besides removing tritium from these purge streams under normal operating conditions, it will have to be capable of (1) handling all plausible forms of high-level tritium release, and (2) providing sufficient enrichment of tritium in protium-contaminated purge-stream effluents to permit the return of tritium to the mainstream fuel cycle. Prospects and economic incentives for various levels of concentration and enrichment of tritium collected by the purges are being evaluated.

7. Blanket-Processing System

This system is essential to Stage II operation. During recent years, considerable attention has been given to tritium recovery from various potential blanket materials; the literature that has evolved on this subject is being reviewed. An attempt is being made to identify, in the broadest sense, all of the blanket processing requirements of a TEPR. Two promising methods for removing tritium from liquid-lithium blankets are being given serious consideration at this time. One involves the removal of tritium (as LiT) and other salt-like impurities (*e.g.*, $Li_3N$, $Li_2C_2$, $Li_2O$) from the lithium blanket by extraction with an appropriately selected molten salt. The second consists of extraction of tritium from liquid lithium in a fluidized bed of a finely divided, solid, hydrogen-gettering material.

## References


1. D. R. Vissers, J. T. Holmes, C. C. McPheeters, L. G. Bartholme, V. M. Kolba, P. A. Nelson, and L. Burris, *Hydrogen-Meter Leak Detector for LMFBR Steam Generators*, USAEC report ANL-8047 (1973).

2. D. R. Vissers, J. T. Holmes, L. G. Bartholme, and P. A. Nelson, Nuclear Technology *12*, 235 (1974).

3. R. H. Armstrong and F. A. Smith, Transactions of the American Nuclear Society *8*, 149 (1965).

4. *Sodium Technology Quarterly Report, January-March, 1970*, USAEC report ANL/ST-2 (1970) p. 5-2.

5. *Sodium Technology Quarterly Report, April-June 1971*, USAEC report ANL-7846 (1971) p. 22.

6. R. Kumar, A. F. Panek, D. J. Raue, and P. A. Nelson, *Continuous Monitors for Tritium in Sodium Coolant and Cover Gas of an LMFBR*, USAEC report ANL-8079 (1974).

7. R. Kumar, *Tritium Transport in an LMFBR*, USAEC report ANL-8089 (1974).

8. E. Berkey *et al.*, Transactions of the American Nuclear Society *12* 609 (1969).

9. *Chemical Engineering Division Physical Inorganic Chemistry Semiannual Report, July-December 1972*, USAEC report ANL-7978 (1972).

10. *Chemical Engineering Division Physical Inorganic Chemistry Semiannual Report, January-June 1973*, USAEC report ANL-8023 (1973).

11. *Chemical Engineering Division Physical Inorganic Chemistry Annual Report, July 1973-June 1974*, USAEC report ANL-8123 (1974).

12. E. Robins, "The Effect of Thermal Gas Motion on Microbalance Measurements," in *Vacuum Microbalance Technique*, Vol. 8, p. 73, Plenum Press, New York (1971).

13. E. Veleckis, E. Van Deventer, and M. Blander, J. Phys. Chem. *78*, 1933 (1974).

14. J. Powell, A. Aronson, P. Belzer, F. Miles, and W. Winsche, "Minimum Activity Blankets Using Aluminum Structure," Proceedings of the First Topical Meeting on the Technology of Controlled Nuclear Fusion, San Diego, April 16-18, 1974, USAEC report CONF-740402, p. 533 (1974).

15. High Performance Batteries for Off-Peak Energy Storage--Progress Report for the Period January-June 1973, USAEC report ANL-8038 (1973).

16. J. Block and A. P. Gray, Inorg. Chem. *4*, 304 (1965).

17. W. McCarty, J. N. Maycock, and V. R. Pai Verneker, J. Phys. Chem. *72*, 4009 (1968).

18. S. Aronson and F. J. Salzano, Inorg. Chem. *8*, 1541 (1969).

19. R. H. Wiswall and E. Wirsing, "Removal of Tritium from Solid CTR Blanket Materials," Proceedings of the ANS Winter Meeting, Washington, D.C., October, 1974.

20. V. A. Maroni, E. J. Cairns and F. A. Cafasso, *A Review of the Chemical, Physical, and Thermal Properties of Lithium That are Related to Its Use in Fusion Reactors*, USAEC report ANL-8001 (1973).

21. K. A. Bolshakov, P. I. Fedorov, and L. A. Stepina, Izvest. Vysshikh Ucheb. Zavedenii, Tsvetnaya Met. *2*, 52 (1959).

22. J. H. Hildebrand and R. L. Scott, *Solubility of Nonelectrolytes*, 3rd ed., Reinhold Publishing Corp., New York (1950) p. 33.

23. *JANAF Thermochemical Tables*, Dow Chemical Company, Midland, Michigan (September, 1966).

24. P. A. G. O'Hare and G. K. Johnson, J. Chem. Thermod. *7*, 13 (1975).

25. D. W. Osborne and H. E. Flotow, Argonne National Laboratory (personal communication).

26. V. A. Maroni, E. Veleckis, and E. H. Van Deventer, "A Review of ANL Research on Lithium-Hydrogen Chemistry and Tritium-Containment Technology," Proceedings of the Symposium on Tritium Technology Related to Fusion Reactor Systems, 1-2 October 1974, Mound Laboratory, Miamisburg, Ohio, USERDA report ERDA-50 (1975).

27. R. L. Leven and R. E. Stickney, "Permeation of Hydrogen Isotopes Through Fusion Reactor Materials," Proc. Fifth Symposium on Engineering Problems of Fusion Research, Princeton University, 6-9 November 1973, IEEE Publication No. 73CH0843-3NPA (1974) p. 212.

28. V. A. Maroni, E. H. Van Deventer, T. A. Renner, R. H. Pelto, and C. J. Wierdak, "Experimental Studies of Tritium Barrier Concepts For Fusion Reactors," Proceedings of the International Conference on Radiation Effects and Tritium Technology for Fusion Reactors, 1-3 October 1975, Gatlinburg, Tennessee.

29. W. G. Perkins and D. R. Begeal, "Permeation and Diffusion of Hydrogen in Ceramvar, Copper, and Ceramvar-Copper Laminates," USAEC report SC-DC-714493 (Sandia Laboratories, March, 1972).

30. F. M. Ehrmann, P. S. Gajardo, and S. C. Droguett, J. Phys. Chem. *77*, 2146 (1973).

31. C. J. Smithells and C. E. Ransley, Proc. Roy. Soc. *150A*, 172 (1935).

32. Yu. I. Belyakov and Yu. I. Zvezdin, Uch. Zap. Leningrad Gos. Univ. Ser. Fiz. Nauk. *No. 345*, 44 (1968).

33. V. A. Maroni, "An Analysis of Tritium Distribution and Leakage Characteristics for Two Fusion Reaction Reference Designs," Proceedings of the Fifth Symposium on Engineering Problems of Fusion Research, IEEE Publication No. 73CH0843-3-NPS (1974), p. 206.

34. W. M. Stacey *et al.*, "Tokamak Experimental Power Reactor Design Studies," Argonne National Laboratory Report ANL-CTR-75-2 (June, 1975).